mathematics

MDPI

Article

Partial Slip Effects for Thermally Radiative Convective Nanofluid Flow

Remus-Daniel Ene [1,†], Nicolina Pop [2,*,†] and Rodica Badarau [3,†]

[1] Department of Mathematics, Politehnica University of Timisoara, 300006 Timisoara, Romania; remus.ene@upt.ro
[2] Department of Physical Foundations of Engineering, Politehnica University of Timisoara, 2 Vasile Parvan Blvd., 300223 Timisoara, Romania
[3] Department of Mechanical Machines, Equipment and Transportation, Politehnica University of Timisoara, 1 Mihai Viteazul Blvd., 300222 Timisoara, Romania; rodica.badarau@upt.ro
* Correspondence: nicolina.pop@upt.ro
† These authors contributed equally to this work.

Abstract: The partial slip effects for radiative convective nanofluid flow over a stretching sheet in porous medium are analytically explored in this work. The Navier–Stokes equations, the momentum and the energy equations are converted into a set of non-linear ODEs by the similarity transformation. Using the modified optimal homotopy asymptotic method (OHAM), the resulting non-linear ODEs are analytically approximately solved. The impact of various parameters, such as: the velocity exponential factor n, the wall thickness parameter γ, the dimensionless velocity slip parameter δ_1, the Prandtl number Pr, the radiation parameter R, and the dimensionless temperature jump parameter δ_2, on the behaviour of the mass and heat transfer is presented. The influence of these parameters is tabular and graphically presented. An excellent agreement between the approximate analytical solution and the corresponding numerical solution is highlighted. The results obtained confirm that modified OHAM is a useful and competitive mathematical tool to explore a large class of non-linear problems with applications in various fields of science and engineering.

Keywords: fluid flow; radiation heat transfer; nanofluid; approximate solution; modified optimal homotopy asymptotic method

MSC: 34A25; 65L99; 76A05; 76D05; 76D10

Citation: Ene, R.-D.; Pop, N.; Badarau, R. Partial Slip Effects for Thermally Radiative Convective Nanofluid Flow. *Mathematics* **2023**, *11*, 2199. https://doi.org/10.3390/math11092199

Academic Editor: Livija Cveticanin

Received: 30 March 2023
Revised: 20 April 2023
Accepted: 5 May 2023
Published: 6 May 2023

1. Introduction

The study of the nanofluid flow has gained considerable attention in recent decades due to its importance in many industrial applications, especially in nanotechnology.

Nanofluids are fluids that contain nanoparticles with superior thermal conductivity properties (silver, copper, iron, carbon nanotubes, CuO, SiO, etc.) in suspension. The aim of using nanofluids is to significantly improve heat transfer by increasing the thermal conductivity of base fluids (ethylene glycol, water, motor oil, acetone, etc.). Solving the equations that characterize nanofluids is important because they govern a very important class of common physical processes. Computational techniques and new approximation methods have made it possible to solve these equations with increasing accuracy, confirming experimental results in broad engineering fields such as: industrial manufacturing processes in the industry of materials with plastic behaviour (extrusion of polymers, spinning of polymer fibres, fibre spinning and drawing plastic films), metal casting, hot rolling, metal spinning, paper manufacture, glass blowing, etc. The equations are also used to model physical phenomena related to fluid flow in the boundary layer, flow processes in porous media with applications in wastewater treatment systems and soil de-pollution in drying beds, in the mining industry.

Many researchers have carried out both experimental and theoretical approaches concerning the boundary layer and heat transfer over a stretching sheet.

In recent years several analytical methods for solving the non-linear differential problem have been used to model the heat and mass transfer in a viscous fluid/nanofluid flow [1–7] were applied.

Vishalakshi et al. [1] obtained the closed-form exact solutions of highly non-linear differential equations of the Walters' liquid B flow. The mass transfer of a chemically reactive species and the flow of MHD over a stretching plate subjected to an inclined magnetic field were examined by Maranna et al. [2]. Sarma et al. [3] explored the exact solution to the problem of a free convective, radiative, viscous, chemically reacting, heat absorbing, incompressible, and unsteady MHD flow using the Laplace transformation technique.

Mahabaleshwar et al. [4] and Akhtar et al. [5] developed novel mathematical techniques to build analytical solutions to non-Newtonian Casson fluid flow.

The velocity and thermal slips of MHD boundary layer flow of Williamson nanofluid was numerically discussed by Reddy et al. [8]. On the other hand, some methods have given numerical solutions. Abbas et al. [9] proposed a model in terms of partial differential equations to study the influence of the Darcy–Forchheimer relation on third-grade fluid flow and heat transfer taking into account the applied magnetic field, Joule heating, thermal diffusion, viscous dissipation, and diffusion-thermo effects. Elbashbeshy et al. [10] analysed the boundary layer flow of a nanofluid containing gyrotactic microorganisms over a vertical stretching surface. Nuwairan et al. [11] explored a model governing a Maxwell nanofluid flow with the effect of activation energy with addition of heat generation/absorption and thermal radiation. Abbas et al. [12] examined the hybrid nanofluid flow past a permeable curved surface with non-linear stretching with injection/suction. Hossein et al. [13] examined the effects of progressive developments in cross-section design, the fuel cell structure, the output current densities and the flooding phenomenon using the finite volume method, and so on [14–38].

In the present work, the modified optimal homotopy asymptotic method (OHAM [39–45] is used to obtain the effective and accurate analytic approximate solutions. This procedure does not depend on small or large parameters and gives us a simple way to optimally control the convergence of approximate solutions using a single iteration.

Our paper is organized as: The introduction is followed by a brief description of the theoretical approach including the steps of the modified OHAM technique in Section 2. Section 3 presents the heat and mass transfer problem by the modified OHAM. The results and some interesting discussions about the effects of non-linear stretching on the flow and heat transfer characteristics are highlighted in Section 4. Conclusions are presented the last section of this paper.

2. Theoretical Approach

2.1. Equations of Motion

The Navier slip conditions are considered for a steady two-dimensional, incompressible, laminar, hydrodynamic flow of a nano fluid over a stretching sheet with non-uniform thickness in porous medium. The sheet is along the x-axis direction and y-axis is normal to it. A non-uniform permeability $K(x) = k_0\ (x+a)^{1-n}$, $n \neq 1$ along with the thermal radiation effect is taken into account. Viscous dissipation effect is neglected in this study. It is assumed that the sheet is stretched with the velocity $u_w(x) = u_0\ (x+a)^n$, $n \neq 1$ and the wall temperature $T_w(x) = T_\infty + T_0\ (x+a)^{(1-n)/2}$, $n \neq 1$. Since the sheet is non-uniform it is assumed that $y = A\ (x+a)^{(1-n)/2}$, $n \neq 1$, where A is the coefficient related to stretching sheet and chosen as a small constant to avoid the external pressure. At $n = 1$ the problem refers flat stretching sheet case.

The physical model is schematically presented in Figure 1.

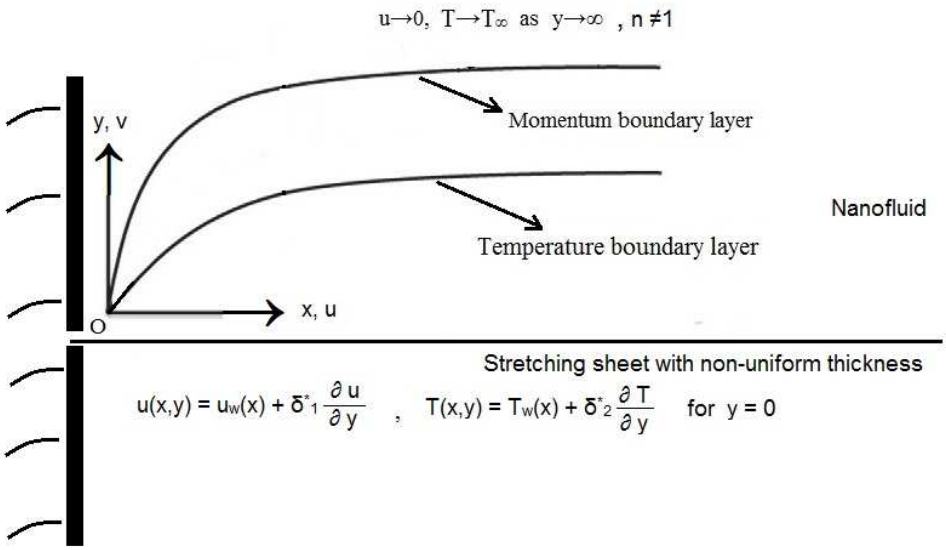

Figure 1. Schematic diagram of the physical model.

As per the above assumptions the governing boundary layer equations are given as follows [46,47]:

$$\frac{\partial u}{\partial x} + \frac{\partial v}{\partial y} = 0, \tag{1}$$

$$u\,\frac{\partial u}{\partial x} + vs.\,\frac{\partial u}{\partial y} = \nu_f\,\frac{\partial^2 u}{\partial y^2}, \tag{2}$$

$$u\,\frac{\partial T}{\partial x} + vs.\,\frac{\partial T}{\partial y} = \alpha\,\frac{\partial^2 T}{\partial y^2} - \frac{1}{(\rho c_p)_f}\cdot\frac{\partial q_r}{\partial y}. \tag{3}$$

The boundary conditions are as follows:

$$\left.\begin{array}{l} u(x,y) = u_w(x) + \delta_1^*\frac{\partial u}{\partial y}, \quad v(x,y) = 0, \\ T(x,y) = T_w(x) + \delta_2^*\frac{\partial T}{\partial y} \end{array}\right\} \text{ at } y = 0, \\ u(x,y) \to 0, \quad T(x,y) \to T_\infty, \quad n \neq 1, \quad \text{at } y \to \infty, \tag{4}$$

where u and v are the velocity components along the x and y directions, respectively, ν_f is the kinematic viscosity, T is the temperature of the fluid, k is the thermal conductivity, α is the thermal diffusivity of the nanofluid, $(\rho c_p)_f$ is the specific heat capacitance, δ_1^* is the dimensional velocity slip parameter and δ_2^* is dimensional temperature jump parameter, these are given by $\delta_1^* = \left(\frac{2-b}{b}\right)\xi_1\,(x+a)^{(1-n)/2}$, $\delta_2^* = \left(\frac{2-c}{c}\right)\xi_2\,(x+a)^{(1-n)/2}$, $\xi_2 = \left(\frac{2\lambda}{\lambda+1}\right)\frac{\xi_1}{Pr}$. Here ξ_1 and ξ_2 are mean free paths and λ is the ratio of specific heats, b and c, respectively, indicating Maxwell's reflection coefficient and thermal accommodation coefficient.

The radiative heat flux q_r under the Rosseland approximation has the form [48]:

$$q_r = -\frac{4\sigma^*}{3k^*}\cdot\frac{\partial T^4}{\partial y}, \tag{5}$$

where σ^* is the Stefan–Boltzmann constant and k^* is the mean absorption coefficient. The temperature differences within the flow are assumed to be sufficiently small such that T^4

may be expressed as a linear function of temperature. Expanding T^4 using a Taylor series and neglecting higher-order terms yields

$$T^4 \cong 4T_\infty^3 T - 3T_\infty^4. \tag{6}$$

The governing Equations are converted into a set of non-linear ordinary differential equations by means of the following similarity transformation [46,47]:

$$\psi(x,y) = \left(\frac{2\nu_f u_0}{n+1}\right)^{1/2} \cdot (x+a)^{(n+1)/2} \cdot f(\eta), \quad \eta = \left(\frac{(n+1)u_0}{2\nu_f}\right)^{1/2} \cdot (x+a)^{(n-1)/2} \cdot y, \quad n \neq 1, \theta(\eta) = \frac{T-T_\infty}{T_w(x)-T_\infty}, \tag{7}$$

where $\psi(x,y)$ is a stream function which satisfies the continuity Equation (1) with

$$u = \frac{\partial\psi(x,y)}{\partial y} \text{ and } vs. = -\frac{\partial\psi(x,y)}{\partial x}. \tag{8}$$

Taking into account of Equations (5)–(8), Equations (2) and (3) become:

$$f''' + ff'' - \left(\frac{2n}{n+1}\right)(f')^2 = 0, \tag{9}$$

$$\frac{1}{Pr}\left(1 + \frac{4}{3}R\right)\theta'' - \left(\frac{1-n}{1+n}\right) f'\theta + f\theta' = 0, \tag{10}$$

with the transformed boundary conditions

$$\begin{aligned} &f(0) = \gamma\left(\frac{1-n}{1+n}\right)[1 + \delta_1 \cdot f''(0)], \quad f'(0) = 1 + \delta_1 \cdot f''(0), \\ &\theta(0) = 1 + \delta_2 \cdot \theta'(0), \quad f'(\infty) \to 0, \quad \theta(\infty) \to 0, \quad n \neq 1, \end{aligned} \tag{11}$$

where $\gamma = A \cdot \left(\frac{(n+1)u_0}{2\nu_f}\right)^{1/2}$, $\delta_1 = \left(\frac{2-b}{b}\right) \cdot \xi_1 \cdot \left(\frac{(n+1)u_0}{2\nu_f}\right)^{1/2}$, $\delta_2 = \left(\frac{2-c}{c}\right) \cdot \xi_2 \cdot \left(\frac{(n+1)u_0}{2\nu_f}\right)^{1/2}$, the prime indicates the differentiation with respect to η, $Pr = \nu_f/\alpha$ is the Prandtl number, $R = \frac{4\sigma T_\infty^3}{kk^*}$ is the radiation parameter, n is the velocity power index parameter, γ is the wall thickness parameter, δ_1 is the dimensionless velocity slip parameter, and δ_2 is the dimensionless temperature jump parameter.

For engineering the shear stress coefficient or friction factor (C_f) and local Nusselt number (Nu_x) are given by

$$Re_x^{0.5} C_f = 2\left(\frac{n+1}{2}\right)^{0.5} f''(0)\,,$$

and

$$Re_x^{-0.5} Nu_x = -\left(\frac{n+1}{2}\right)^{0.5} \theta'(0)\,,$$

where $Re_x = \frac{u_w(x+a)}{\nu_f}$ is the local Reynolds number.

2.2. Steps of the Modified Optimal Homotopy Asymptotic Method (OHAM)

The OHAM technique [39] has the following steps:

(i) The non-linear differential equation has the general form:

$$\mathcal{L}\Big(F(\eta)\Big) + \mathcal{N}\Big(F(\eta)\Big) = 0, \tag{12}$$

with the boundary/initial conditions

$$\mathcal{B}\left(F(\eta), \frac{dF(\eta)}{d\eta}\right) = 0, \tag{13}$$

where $\mathcal{L}\left(F(\eta)\right)$ and $\mathcal{N}\left(F(\eta)\right)$ describe the linear part and the non-linear part, respectively, and $\mathcal{B}$ is an operator describing the boundary conditions, while $F(\eta)$ is the unknown smooth function.

(ii) The homotopic relation is given by:

$$\mathcal{H}\left[\mathcal{L}\left(F(\eta,p)\right),\ H(\eta,C_i),\ \mathcal{N}\left(F(\eta,p)\right)\right] = \mathcal{L}\left(F_0(\eta)\right) + G(\eta) + p\left[\mathcal{L}\left(F_1(\eta,C_i)\right) - H(\eta,C_i)\mathcal{N}\left(F_0(\eta)\right)\right], \tag{14}$$

where $G(\eta)$ is a known function, $p \in [0,\ 1]$ is the embedding parameter and $H(\eta,C_i) \neq 0$ is an auxiliary convergence-control function depending on the variable η, the parameters C_1, C_2, ..., C_s, and choosing the unknown function $F(\eta)$ in the form:

$$F(\eta,p) = F_0(\eta) + pF_1(\eta,C_i), \tag{15}$$

and by equating the coefficients of p^0 and p^1, respectively, yields:
the zeroth-order deformation problem

$$\mathcal{L}\left(F_0(\eta)\right) + G(\eta) = 0, \quad \mathcal{B}\left(F_0(\eta), \frac{dF_0(\eta)}{d\eta}\right) = 0, \tag{16}$$

the first-order deformation problem

$$\begin{aligned} &\mathcal{L}\left(F_1(\eta,C_i)\right) = H(\eta,C_i)\mathcal{N}\left(F_0(\eta)\right), \\ &\mathcal{B}\left(F_1(\eta,C_i), \tfrac{dF_1(\eta,C_i)}{d\eta}\right) = 0, \ \ i = 1,2,...,s. \end{aligned} \tag{17}$$

(iii) The initial approximation $F_0(\eta)$ can be obtained by solving the linear Equation (16).

(iv) In order to compute $F_1(\eta,C_i)$ by Equation (17), for the non-linear operator $\mathcal{N}$ was chosen general form

$$\mathcal{N}(F_0(\eta)) = \textstyle\sum_{i=1}^{n} h_i(\eta)g_i(\eta), \tag{18}$$

where n is a positive integer, and $h_i(\eta)$ and $g_i(\eta)$ are known elementary functions that depend on $F_0(\eta)$ and $\mathcal{N}$.

The computation of the first approximation $F_1(\eta,C_i)$ leads to:

$$F_1(\eta,C_i) = \textstyle\sum_{i=1}^{m} H_i(\eta,h_j(\eta),C_j)g_i(\eta), \quad j = 1,\ ...,\ s, \tag{19}$$

or

$$\begin{aligned} &F_1(\eta,C_i) = \textstyle\sum_{i=1}^{m} H_i(\eta,g_j(\eta),C_j)h_i(\eta), \quad j = 1,\ ...,\ s, \\ &\mathcal{B}\left(F_1(\eta,C_i),\ \tfrac{dF_1(\eta,C_i)}{d\eta}\right) = 0. \end{aligned} \tag{20}$$

The above expressions of $H_i(\eta,h_j(\eta),C_j)$ contain linear combinations of the elementary functions h_j, $j = 1,\ ...,\ s$ and the parameters C_j, $j = 1,\ ...,\ s$. The summation limit m is an arbitrary positive integer.

(v) The first-order analytical approximate solutions of Equations (12) and (13), taking into account Equation (15), could be written as:

$$\overline{F}(\eta,C_i) = F(\eta,1) = F_0(\eta) + F_1(\eta,C_i). \tag{21}$$

The convergence-control parameters C_1, C_2, ..., C_s can be optimally identified by various methods, such as: the Kantorowich method, the collocation method, the Galerkin method, the least square method, or the weighted residual method.

Therefore, in this case we construct an analytic approximate solution using the modified optimal homotopy asymptotic method (OHAM).

3. Heat and Mass Transfer Problem by the Modified OHAM

OHAM procedure will be apply in order to obtain approximate solutions to Equations (9) and (10) with the initial/boundary conditions in Equation (11).

For this purpose, for the non-linear Equation (9), we choose the linear operator of the form:

$$\mathcal{L}_f(\eta) = f'''(\eta) - K_1^2 f'(\eta) + G(\eta), \tag{22}$$

where the given arbitrary function $G(\eta) = ae^{-K_2\eta} + c_1e^{-K_0\eta} + c_2e^{-2K_0\eta} + c_3e^{-3K_0\eta}$ and K_0, K_1, K_2, a, c_1, c_2, c_3 are some unknown positive parameters to be determined later.

The initial approximation $f_0(\eta)$ can be obtained from the following problem:

$$\begin{aligned} &f_0'''(\eta) - K_1^2 f_0'(\eta) + G(\eta) = 0, \\ &f_0(0) = \gamma \cdot \tfrac{1-n}{1+n} \cdot f_0'(0), \quad f_0'(0) = 1 + \delta_1 f_0''(0), \quad f_0'(\infty) = 0, \end{aligned} \tag{23}$$

with the solution:

$$f_0(\eta) = b_0 + b_1e^{-K_1\eta} + b_2e^{-K_2\eta} + d_1e^{-K_0\eta} + d_2e^{-2K_0\eta} + d_3e^{-3K_0\eta}\ , \tag{24}$$

where

$$d_1 = \frac{c_1}{K_0^3 - K_0K_1^2},\ d_2 = \frac{c_2}{8K_0^3 - 2K_0K_1^2},\ d_3 = \frac{c_3}{27K_0^3 - 3K_0K_1^2},\ b_2 = \frac{a}{K_2^3 - K_2K_1^2},$$

$$b_1 = -\frac{1}{K_1^2 + K_1} \cdot \left[1 + \frac{a(1+K_2)}{K_2^2 - K_1^2} + \frac{c_1(1+K_0)}{K_0^2 - K_1^2} + \frac{c_2(1+2K_0)}{4K_0^2 - K_1^2} + \frac{c_3(1+3K_0)}{9K_0^2 - K_1^2}\right],$$

$$b_0 = \gamma\frac{1-n}{1+n} \cdot \Big(- b_1K_1 - b_2K_2 - d_1K_0 - 2d_2K_0 - 3d_3K_0\Big) - b_1 - b_2 - d_1 - d_2 - d_3\ .$$

The non-linear operator $\mathcal{N}_f(\eta)$, corresponding to the non-linear differential Equation (9), is defined by:

$$\mathcal{N}_f\Big(\eta\Big) = ff'' - \tfrac{2n}{n+1}(f')^2 + K_1^2\, f'\ . \tag{25}$$

For the initial approximation $f_0(\eta)$ given by Equation (24), the non-linear operator Equation (25) becomes:

$$\begin{aligned} &\mathcal{N}_{f_0}(\eta) = f_0f_0'' - \tfrac{2n}{n+1}(f_0')^2 + K_1^2\, f_0' = \\ &= m_1e^{-K_0\eta} + m_2e^{-2K_0\eta} + m_3e^{-3K_0\eta} + m_4e^{-4K_0\eta} + m_5e^{-5K_0\eta} + m_6e^{-6K_0\eta} + m_7e^{-K_1\eta} + \\ &+ m_8e^{-2K_1\eta} + m_9e^{-K_2\eta} + m_{10}e^{-2K_2\eta} + m_{11}e^{-(K_1+K_0)\eta} + m_{12}e^{-(K_1+2K_0)\eta} + m_{13}e^{-(K_1+3K_0)\eta} + \\ &+ m_{14}e^{-(K_2+K_0)\eta} + m_{15}e^{-(K_2+2K_0)\eta} + m_{16}e^{-(K_2+3K_0)\eta} + m_{17}e^{-(K_1+K_2)\eta}\ , \end{aligned} \tag{26}$$

where

$$m_1 = b_0d_1K_0^2 - d_1K_0K_1^2\ ,\ m_2 = d_1^2K_0^2 + 4b_0d_2K_0^2 - d_1^2K_0^2 \cdot \frac{2n}{n+1} - 2d_2K_0K_1^2\ ,$$

$$m_3 = 5d_1d_2K_0^2 + 9b_0d_3K_0^2 - 4d_1d_2K_0^2 \cdot \frac{2n}{n+1} - 3d_3K_0K_1^2\ ,$$

$$m_4 = 4d_2^2K_0^2 + 10d_1d_3K_0^2 - 4d_2^2K_0^2 \cdot \frac{2n}{n+1} - 6d_1d_3K_0^2 \cdot \frac{2n}{n+1}\ ,$$

$$m_5 = 13d_2d_3K_0^2 - 12d_2d_3K_0^2 \cdot \frac{2n}{n+1}\ ,\ m_6 = 9d_3^2K_0^2 - 9d_3^2K_0^2 \cdot \frac{2n}{n+1}\ ,$$

$$m_7 = b_0b_1K_1^2 - b_1K_1^3\ ,\ m_8 = b_1^2K_1^2 - b_1^2K_1^2 \cdot \frac{2n}{n+1}\ ,$$

$$m_9 = b_0 b_2 K_2^2 - b_2 K_2 K_1^2 \, , m_{10} = b_2^2 K_2^2 - b_2^2 K_2^2 \cdot \frac{2n}{n+1} \, ,$$
$$m_{11} = b_1 d_1 K_0^2 + b_1 d_1 K_1^2 - 2 b_1 d_1 K_0 K_1 \cdot \frac{2n}{n+1} \, ,$$
$$m_{12} = 4 b_1 d_2 K_0^2 + b_1 d_2 K_1^2 - 4 b_1 d_2 K_0 K_1 \cdot \frac{2n}{n+1} \, ,$$
$$m_{13} = 9 b_1 d_3 K_0^2 + b_1 d_3 K_1^2 - 6 b_1 d_2 K_0 K_1 \cdot \frac{2n}{n+1} \, ,$$
$$m_{14} = b_2 d_1 K_0^2 + b_2 d_1 K_2^2 - 2 b_2 d_1 K_0 K_2 \cdot \frac{2n}{n+1} \, ,$$
$$m_{15} = 4 b_2 d_2 K_0^2 + b_2 d_2 K_2^2 - 4 b_2 d_2 K_0 K_2 \cdot \frac{2n}{n+1} \, ,$$
$$m_{16} = 9 b_2 d_3 K_0^2 + b_2 d_3 K_2^2 - 6 b_2 d_3 K_0 K_2 \cdot \frac{2n}{n+1} \, ,$$
$$m_{17} = b_1 b_2 K_1^2 + b_1 b_2 K_2^2 - 2 b_1 b_2 \cdot \frac{2n}{n+1} \, .$$

Comparing Equations (18) and (26), one obtains:

$$\begin{array}{llll}
h_1(\eta) = m_1 & , & g_1(\eta) = e^{-K_0 \eta} \\
h_2(\eta) = m_2 & , & g_2(\eta) = e^{-2K_0 \eta} \\
h_3(\eta) = m_3 & , & g_3(\eta) = e^{-3K_0 \eta} \\
h_4(\eta) = m_4 & , & g_4 = e^{-4K_0 \eta} \\
h_5(\eta) = m_5 & , & g_5 = e^{-5K_0 \eta} \\
h_6(\eta) = m_6 & , & g_6 = e^{-6K_0 \eta} \\
h_7(\eta) = m_7 & , & g_7 = e^{-K_1 \eta} + \\
h_8(\eta) = m_8 & , & g_8 = e^{-2K_1 \eta} \\
h_9(\eta) = m_9 & , & g_9 = e^{-K_2 \eta} \\
h_{10}(\eta) = m_{10} & , & g_{10} = e^{-2K_2 \eta} \\
h_{11}(\eta) = m_{11} & , & g_{11} = e^{-(K_1+K_0)\eta} \\
h_{12}(\eta) = m_{12} & , & g_{12} = e^{-(K_1+2K_0)\eta} \\
h_{13}(\eta) = m_{13} & , & g_{13} = e^{-(K_1+3K_0)\eta} \\
h_{14}(\eta) = m_{14} & , & g_{14} = e^{-(K_2+K_0)\eta} \\
h_{15}(\eta) = m_{15} & , & g_{15} = e^{-(K_2+2K_0)\eta} \\
h_{16}(\eta) = m_{16} & , & g_{16} = e^{-(K_2+3K_0)\eta} \\
h_{17}(\eta) = m_{17} & , & g_{17} = e^{-(K_1+K_2)\eta} \, .
\end{array} \tag{27}$$

The first approximation $f_1(\eta)$ given by Equation (19) becomes:

$$\begin{array}{l}
f_1(\eta, C_i) = H_1(\eta, C_i) e^{-K_0 \eta} + H_2(\eta, C_i) e^{-2K_0 \eta} + H_3(\eta, C_i) e^{-3K_0 \eta} + H_4(\eta, C_i) e^{-4K_0 \eta} + \\
+ H_5(\eta, C_i) e^{-5K_0 \eta} + H_6(\eta, C_i) e^{-6K_0 \eta} + H_7(\eta, C_i) e^{-K_1 \eta} + H_8(\eta, C_i) e^{-2K_1 \eta} + H_9(\eta, C_i) e^{-K_2 \eta} + \\
+ H_{10}(\eta, C_i) e^{-2K_2 \eta} + H_{11}(\eta, C_i) e^{-(K_1+K_0)\eta} + H_{12}(\eta, C_i) e^{-(K_1+2K_0)\eta} + H_{13}(\eta, C_i) e^{-(K_1+3K_0)\eta} + \\
+ H_{14}(\eta, C_i) e^{-(K_2+K_0)\eta} + H_{15}(\eta, C_i) e^{-(K_2+2K_0)\eta} + H_{16}(\eta, C_i) e^{-(K_2+3K_0)\eta} + H_{17}(\eta, C_i) e^{-(K_1+K_2)\eta} \, ,
\end{array} \tag{28}$$

where there are many possibilities to choose the convergence-control functions H_i, $i = 1, 2, \cdots, 17$ as follows (see Marinca and Herisanu [39]):

$$\begin{array}{l}
H_1(\eta, C_i) = C_1 \eta^2 + C_2 \eta^3 + C_3 \eta^4 \, , \; H_2(\eta, C_i) = (C_4 \eta^2 + C_5 \eta^3) \cdot e^{-\alpha_1 \eta} \, , \\
H_3(\eta, C_i) = (C_6 \eta^2 + C_7 \eta^3) \cdot e^{-\alpha_2 \eta} \, , \; H_4(\eta, C_i) = (C_8 \eta^2 + C_9 \eta^3) \cdot e^{-\alpha_3 \eta} \, , \\
H_5(\eta, C_i) = (C_{10} \eta^2 + C_{11} \eta^3) \cdot e^{-\alpha_4 \eta} \, , \; H_6(\eta, C_i) = (C_{12} \eta^2 + C_{13} \eta^3) \cdot e^{-\alpha_5 \eta} \, , \\
H_7(\eta, C_i) = \cdots = H_{17}(\eta, C_i) = 0
\end{array} \tag{29}$$

with $C_1 = -(C_{10} + C_{12} + C_4 + C_6 + C_8)$, $\alpha_1 > 0$, $\alpha_2 > 0$, $\alpha_3 > 0$, $\alpha_4 > 0$, $\alpha_5 > 0$.

Inserting Equation (29) into Equation (28) results:

$$f_1(\eta, C_i) = (C_1\eta^2 + C_2\eta^3 + C_3\eta^4)e^{-K_0\eta} + (C_4\eta^2 + C_5\eta^3)e^{-(\alpha_1+2K_0)\eta} + (C_6\eta^2 + C_7\eta^3)e^{-(\alpha_2+3K_0)\eta} + \\ +(C_8\eta^2 + C_9\eta^3)e^{-(\alpha_3+4K_0)\eta} + (C_{10}\eta^2 + C_{11}\eta^3)e^{-(\alpha_4+5K_0)\eta} + (C_{12}\eta^2 + C_{13}\eta^3)e^{-(\alpha_5+6K_0)\eta}\,. \tag{30}$$

The first-order approximate solution given by Equation (21) is obtained from Equations (24) and (30):

$$\overline{f}(\eta, C_i) = f_0(\eta) + f_1(\eta, C_i) = b_0 + b_1e^{-K_1\eta} + b_2e^{-K_2\eta} + d_1e^{-K_0\eta} + d_2e^{-2K_0\eta} + d_3e^{-3K_0\eta} + \\ +(C_1\eta^2 + C_2\eta^3 + C_3\eta^4)e^{-K_0\eta} + (C_4\eta^2 + C_5\eta^3)e^{-(\alpha_1+2K_0)\eta} + (C_6\eta^2 + C_7\eta^3)e^{-(\alpha_2+3K_0)\eta} + \\ +(C_8\eta^2 + C_9\eta^3)e^{-(\alpha_3+4K_0)\eta} + (C_{10}\eta^2 + C_{11}\eta^3)e^{-(\alpha_4+5K_0)\eta} + (C_{12}\eta^2 + C_{13}\eta^3)e^{-(\alpha_5+6K_0)\eta}\,. \tag{31}$$

where the unknown constants C_i, $i = 1, \cdots, 13$, $b_0, b_1, b_2, d_1, d_2, d_3, K_0 > 0, K_1 > 0, K_2 > 0$, $\alpha_1 > 0, \alpha_2 > 0, \alpha_3 > 0, \alpha_4 > 0, \alpha_5 > 0$ will be optimally identified, with $K_0 \neq K_1 \neq K_2$.

In this way, other approximate analytic solutions could be found.

The linear operator $\mathcal{L}_\theta(\eta)$ for Equation (10), with initial/boundary conditions given by Equation (11) (for the unknown function θ), is chosen as:

$$\mathcal{L}_\theta(\eta) = \theta'' - K_3^2\theta, \tag{32}$$

where $K_3 > 0$ is an unknown parameter at this moment.

Equation (16) can be written in the form:

$$\theta_0'' - K_3^2\theta_0 = 0, \quad \theta_0(0) = 1 + \delta_2\theta_0'(0), \quad \theta_0(\infty) = 0 \tag{33}$$

and has the solution

$$\theta_0(\eta) = \frac{1}{1 + K_3\delta_2}e^{-K_3\eta}. \tag{34}$$

The non-linear operator $\mathcal{N}_\theta$ corresponding to the unknown function θ is obtained from the expression Equation (10) in the form:

$$\mathcal{N}_\theta(\eta) = K_3^2\theta + \frac{Pr}{1 + \frac{4}{3}R}\left(f\theta' - \frac{1-n}{1+n}f'\theta\right). \tag{35}$$

For the initial approximation $\theta_0(\eta)$ given by Equation (34), the non-linear operator Equation (35) becomes:

$$\mathcal{N}_{\theta_0}(\eta) = K_3^2\theta_0 + \frac{Pr}{1+\frac{4}{3}R}\left(f\theta_0' - \frac{1-n}{1+n}f'\theta_0\right) = \\ = \frac{K_3^2}{1+K_3\delta_2}e^{-K_3\eta} + \frac{Pr}{1+\frac{4}{3}R}\left(-\frac{K_3}{1+K_3\delta_2}\cdot f\cdot e^{-K_3\eta} - \frac{1-n}{1+n}\cdot\frac{1}{1+K_3\delta_2}\cdot f'\cdot e^{-K_3\eta}\right), \tag{36}$$

where $f(\eta)$ is given by Equation (31).

In comparing Equations (18) and (36) one can obtain:

$$
\begin{aligned}
&h_1^*(\eta) = \tfrac{K_3^2}{1+K_3\delta_2} - \tfrac{b_0K_3}{1+K_3\delta_2}\cdot\tfrac{Pr}{1+\frac{4}{3}R},\ \ g_1^*(\eta) = e^{-K_3\eta},\\
&h_2^*(\eta) = \Big(-\tfrac{b_1K_3}{1+K_3\delta_2} + \tfrac{b_1K_1}{1+K_3\delta_2}\cdot\tfrac{1-n}{1+n}\Big)\cdot\tfrac{Pr}{1+\frac{4}{3}R},\ \ g_2^*(\eta) = e^{-(K_1+K_3)\eta},\\
&h_3^*(\eta) = \Big(-\tfrac{b_2K_3}{1+K_3\delta_2} + \tfrac{b_2K_2}{1+K_3\delta_2}\cdot\tfrac{1-n}{1+n}\Big)\cdot\tfrac{Pr}{1+\frac{4}{3}R},\ \ g_3^*(\eta) = e^{-(K_2+K_3)\eta},\\
&h_4^*(\eta) = \Big[-K_3\cdot(d_1+C_1\eta^2+C_2\eta^3+C_3\eta^4) + K_0\cdot(d_1+C_1\eta^2+C_2\eta^3+C_3\eta^4)\cdot\tfrac{1-n}{1+n} -\\
&-(2C_1\eta+3C_2\eta^2+4C_3\eta^3)\cdot\tfrac{1-n}{1+n}\Big]\cdot\tfrac{Pr}{1+\frac{4}{3}R}\cdot\tfrac{1}{1+K_3\delta_2},\ \ g_4^*(\eta) = e^{-(K_0+K_3)\eta},\\
&h_5^*(\eta) = \Big(-\tfrac{d_2K_3}{1+K_3\delta_2} + \tfrac{2d_2K_0}{1+K_3\delta_2}\cdot\tfrac{1-n}{1+n}\Big)\cdot\tfrac{Pr}{1+\frac{4}{3}R},\ \ g_5^*(\eta) = e^{-(2K_0+K_3)\eta},\\
&h_6^*(\eta) = \Big(-\tfrac{d_3K_3}{1+K_3\delta_2} + \tfrac{3d_3K_0}{1+K_3\delta_2}\cdot\tfrac{1-n}{1+n}\Big)\cdot\tfrac{Pr}{1+\frac{4}{3}R},\ \ g_6^*(\eta) = e^{-(3K_0+K_3)\eta},\\
&h_7^*(\eta) = \Big[-K_3\cdot(C_4\eta^2+C_5\eta^3) + (\alpha_1+2K_0)\cdot(C_4\eta^2+C_5\eta^3)\cdot\tfrac{1-n}{1+n} -\\
&-(2C_4\eta+3C_5\eta^2)\cdot\tfrac{1-n}{1+n}\Big]\cdot\tfrac{Pr}{1+\frac{4}{3}R}\cdot\tfrac{1}{1+K_3\delta_2},\ \ g_7^*(\eta) = e^{-(\alpha_1+2K_0+K_3)\eta},\\
&h_8^*(\eta) = \Big[-K_3\cdot(C_6\eta^2+C_7\eta^3) + (\alpha_2+3K_0)\cdot(C_6\eta^2+C_7\eta^3)\cdot\tfrac{1-n}{1+n} -\\
&-(2C_6\eta+3C_7\eta^2)\cdot\tfrac{1-n}{1+n}\Big]\cdot\tfrac{Pr}{1+\frac{4}{3}R}\cdot\tfrac{1}{1+K_3\delta_2},\ \ g_8^*(\eta) = e^{-(\alpha_2+3K_0+K_3)\eta},\\
&h_9^*(\eta) = \Big[-K_3\cdot(C_8\eta^2+C_9\eta^3) + (\alpha_3+4K_0)\cdot(C_8\eta^2+C_9\eta^3)\cdot\tfrac{1-n}{1+n} -\\
&-(2C_8\eta+3C_9\eta^2)\cdot\tfrac{1-n}{1+n}\Big]\cdot\tfrac{Pr}{1+\frac{4}{3}R}\cdot\tfrac{1}{1+K_3\delta_2},\ \ g_9^*(\eta) = e^{-(\alpha_3+4K_0+K_3)\eta},\\
&h_{10}^*(\eta) = \Big[-K_3\cdot(C_{10}\eta^2+C_{11}\eta^3) + (\alpha_4+5K_0)\cdot(C_{10}\eta^2+C_{11}\eta^3)\cdot\tfrac{1-n}{1+n} -\\
&-(2C_{10}\eta+3C_{11}\eta^2)\cdot\tfrac{1-n}{1+n}\Big]\cdot\tfrac{Pr}{1+\frac{4}{3}R}\cdot\tfrac{1}{1+K_3\delta_2},\ \ g_{10}^*(\eta) = e^{-(\alpha_4+5K_0+K_3)\eta},\\
&h_{11}^*(\eta) = \Big[-K_3\cdot(C_{12}\eta^2+C_{13}\eta^3) + (\alpha_5+6K_0)\cdot(C_{12}\eta^2+C_{13}\eta^3)\cdot\tfrac{1-n}{1+n} -\\
&-(2C_{12}\eta+3C_{13}\eta^2)\cdot\tfrac{1-n}{1+n}\Big]\cdot\tfrac{Pr}{1+\frac{4}{3}R}\cdot\tfrac{1}{1+K_3\delta_2},\ \ g_{11}^*(\eta) = e^{-(\alpha_5+6K_0+K_3)\eta}.
\end{aligned}
\tag{37}
$$

The first approximation $\theta_1(\eta, D_i)$, given by Equation (19), becomes:

$$
\begin{aligned}
&\theta_1(\eta,D_i) = H_1^*(\eta,D_i)\cdot e^{-K_3\eta} + H_2^*(\eta,D_i)\cdot e^{-(K_1+K_3)\eta} + H_3^*(\eta,D_i)\cdot e^{-(K_2+K_3)\eta} +\\
&+H_4^*(\eta,D_i)\cdot e^{-(K_0+K_3)\eta} + H_5^*(\eta,D_i)\cdot e^{-(2K_0+K_3)\eta} + H_6^*(\eta,D_i)\cdot e^{-(3K_0+K_3)\eta} +\\
&+H_7^*(\eta,D_i)\cdot e^{-(\alpha_1+2K_0+K_3)\eta} + H_8^*(\eta,D_i)\cdot e^{-(\alpha_2+3K_0+K_3)\eta} + H_9^*(\eta,D_i)\cdot e^{-(\alpha_3+4K_0+K_3)\eta} +\\
&+H_{10}^*(\eta,D_i)\cdot e^{-(\alpha_4+5K_0+K_3)\eta} + H_{11}^*(\eta,D_i)\cdot e^{-(\alpha_5+6K_0+K_3)\eta},
\end{aligned}
\tag{38}
$$

where D_i are unknown parameters, and the unknown auxiliary functions $H_1^*(\eta, D_i)$, ..., $H_5^*(\eta, D_i)$ can be of the form:

$$
\begin{aligned}
&H_1^*(\eta,D_i) = D_0\eta,\ \ H_2^*(\eta,D_i) = D_1+D_2\eta+D_3\eta^2,\ \ H_3^*(\eta,D_i) = D_4+D_5\eta+D_6\eta^2,\\
&H_4^*(\eta,D_i) = D_7\ \ ,\ \ H_5^*(\eta,D_i) = D_8+D_9\eta+D_{10}\eta^2\ \ ,\ \ H_6^*(\eta,D_i) = \cdots = H_{11}^*(\eta,D_i) = 0\,.
\end{aligned}
\tag{39}
$$

Inserting Equation (39) into Equation (38) one obtains:

$$\theta_1(\eta, D_i) = D_0\eta \cdot e^{-K_3\eta} + (D_1 + D_2\eta + D_3\eta^2) \cdot e^{-(K_1+K_3)\eta} + (D_4 + D_5\eta + D_6\eta^2) \cdot e^{-(K_2+K_3)\eta} + \\ + D_7 \cdot e^{-(K_0+K_3)\eta} + (D_8 + D_9\eta + D_{10}\eta^2) \cdot e^{-(2K_0+K_3)\eta}\ , \tag{40}$$

with $D_7 = -D_1 - D_4 - D_8$.

From Equations (34) and (40), the first-order approximate solution given by Equation (21) has the form:

$$\bar{\theta}(\eta, D_i) = \theta_0(\eta) + \theta_1(\eta, D_i) = \\ = \frac{1}{1 + K_3\delta_2} e^{-K_3\eta} + D_0\eta \cdot e^{-K_3\eta} + (D_1 + D_2\eta + D_3\eta^2) \cdot e^{-(K_1+K_3)\eta} + \\ + (D_4 + D_5\eta + D_6\eta^2) \cdot e^{-(K_2+K_3)\eta} + D_7 \cdot e^{-(K_0+K_3)\eta} + (D_8 + D_9\eta + D_{10}\eta^2) \cdot e^{-(2K_0+K_3)\eta}\ , \tag{41}$$

where the unknown parameters $K_3 > 0$, D_i, $i = 1, \cdots, 10$ are optimally identified.

Taking into account of the analytical approximate solutions $\bar{f}(\eta)$ and $\bar{\theta}(\eta)$ given by the Equations (9) and (10), respectively,the residuals from Equation (31) and (41), respectively, are:

$$R_{\bar{f}}(\eta) = \bar{f}''' + \bar{f}\bar{f}'' - \left(\frac{2n}{n+1}\right)(\bar{f}')^2, \tag{42}$$

and

$$R_{\bar{\theta}}(\eta) = \frac{1}{Pr}\left(1 + \frac{4}{3}R\right)\bar{\theta}'' - \left(\frac{1-n}{1+n}\right)\bar{f}'\bar{\theta} + \bar{f}\bar{\theta}'\ . \tag{43}$$

4. Numerical Results and Discussion

By comparison of our approximate solutions with numerical results obtained via the fourth-order Runge–Kutta method in the following cases: $n \in \{0.5, 2.5, 5\}$, $\gamma \in \{0.25, 0.5, 1\}$, $\delta_1 \in \{0.2, 0.5, 0.75\}$, $Pr \in \{6, 7, 8\}$, $R \in \{0.5, 1, 1.5\}$, $\delta_2 \in \{0.2, 0.4, 0.6\}$, demonstrating the advantages of the modified OHAM technique, in terms of accuracy, flexibility, validity and efficiency.

The obtained analytic approximate solutions for the displacement $\bar{f}$ and corresponding velocity $\bar{f}'$, and the temperature $\bar{\theta}$ are presented below. The effects of the different parameters are discussed. The precision of these solutions are shown in Tables 1–4 for the skin-friction coefficient $\bar{f}''(0)$, the heat transfer coefficient $\bar{\theta}'(0)$, the displacement $\bar{f}(\eta)$, the corresponding velocity $\bar{f}'(\eta)$ and the temperature $\bar{\theta}(\eta)$ when $n = 0.5$, $\gamma = 0.25$, $\delta_1 = 0.5$, $R = 1$, $Pr = 6$, $\delta_2 = 0.2$, the limit-value $f(\infty) := \lim_{\eta\to\infty} f(\eta)$.

Table 1. Values of the skin-friction coefficient $\bar{f}''(0)$ obtained from Equation (31) by the OHAM and numerical results, for different values of n, γ and δ_1 (relative errors: $\epsilon_{f''(0)} = |f''_{numerical}(0) - \bar{f}''_{OHAM}(0)|$).

n	γ	δ_1	$f''_{numerical}(0)$	$\bar{f}''_{OHAM}(0)$	$\epsilon_{f''(0)}$
0.5	0.25	0.2	−0.7333855928	−0.7333855918	10^{-9}
0.5	0.25	0.5	−0.5639692215	−0.5639692205	10^{-9}
0.5	0.25	0.75	−0.4764796954	−0.4764796944	10^{-9}
0.5	0.5	0.5	−0.5784360410	−0.5784360310	10^{-8}
0.5	1	0.5	−0.6070808644	−0.6070808634	10^{-9}
2.5	0.25	0.5	−0.6216320348	−0.6216320248	10^{-8}
5	0.25	0.5	−0.6367180731	−0.6367180631	10^{-8}

Table 2. Values of the heat transfer coefficient $\bar{\theta}'(0)$ obtained from Equation (41) by the OHAM and numerical results, for different values of n, γ, δ_1, R, Pr, and δ_2 (relative errors: $\epsilon_{\theta'(0)} = |\theta'_{numerical}(0) - \bar{\theta}'_{OHAM}(0)|$).

n	γ	δ_1	R	Pr	δ_2	$\theta'_{numerical}(0)$	$\bar{\theta}'_{OHAM}(0)$	$\epsilon_{\theta'(0)}$
0.5	0.25	0.5	1	6	0.2	−0.9865380801	−0.9865379801	10^{-7}
0.5	0.25	0.5	1	7	0.2	−1.0639948406	−1.0639947406	10^{-7}
0.5	0.25	0.5	1	8	0.2	−1.1340917886	−1.1340916886	10^{-7}
0.5	0.25	0.5	0.5	6	0.2	−1.1604012664	−1.1604012564	10^{-8}
0.5	0.25	0.5	1	6	0.2	−0.9865380801	−0.9865379801	10^{-7}
0.5	0.25	0.5	1.5	6	0.2	−0.8681344977	−0.8681344877	10^{-8}
0.5	0.25	0.5	1	6	0.2	−0.9865380801	−0.9865379801	10^{-7}
0.5	0.25	0.5	1	6	0.4	−0.8239638179	−0.8239637179	10^{-7}
0.5	0.25	0.5	1	6	0.6	−0.7073908656	−0.7073907656	10^{-7}
2.5	0.25	0.5	1	6	0.2	−0.3797410596	−0.3885966996	$8.855639 \cdot 10^{-3}$
5	0.25	0.5	1	6	0.2	−0.0997737511	−0.0997737411	10^{-8}
0.5	0.5	0.5	1	6	0.2	−1.0438247676	−1.0438246676	10^{-7}
0.5	1	0.5	1	6	0.2	−1.1564371927	−1.1564370927	10^{-7}
0.5	0.25	0.2	1	6	0.2	−1.0625520610	−1.0625520510	10^{-8}
0.5	0.25	0.75	1	6	0.2	−0.9401404517	−0.9401403517	10^{-7}

Table 3. Values of the analytic approximate solutions $\bar{f}(\eta)$ and $\bar{f}'(\eta)$ from Equation (A3) and $\bar{\theta}(\eta)$ from Equation (A4) obtained by the OHAM and corresponding numerical results, for the values $n = 0.5$, $\gamma = 0.25$, $\delta_1 = 0.5$, $R = 1$, $Pr = 6$, and $\delta_2 = 0.2$ (relative errors: $\epsilon_f = |f_{numerical} - \bar{f}_{OHAM}|$, $\epsilon_{f'} = |f'_{numerical} - \bar{f}'_{OHAM}|$, $\epsilon_\theta = |\theta_{numerical} - \bar{\theta}_{OHAM}|$).

η	$f_{numerical}$	$f'_{numerical}$	$\theta_{numerical}$
0	0.0598346157	0.7180153892	0.8026923839
0.25	0.2226712355	0.5883987717	0.5777496315
0.5	0.3557863062	0.4798072617	0.3992585355
0.75	0.4641079810	0.3896154306	0.2660675341
1	0.5519132878	0.3152605148	0.1718011819
1.25	0.6228576040	0.2543456969	0.1079932864
1.5	0.6800247596	0.2047029048	0.0663727087
1.75	0.7259884392	0.1644214653	0.0400386110
2	0.7628774926	0.1318523678	0.0237854503
2.25	0.7924400119	0.1055954914	0.0139544082
2.5	0.8161029111	0.0844773589	0.0081040406
2.75	0.8350253351	0.0675246921	0.0046679539
3	0.8501452478	0.0539367909	0.0026710288
η	$\bar{f}_{OHAM}$	$\bar{f}'_{OHAM}$	$\bar{\theta}_{OHAM}$
0	0.0598346158	0.7180153897	0.8026925039
0.25	0.2226712379	0.5883987726	0.5777441370
0.5	0.3557863072	0.4798072319	0.3992654139
0.75	0.4641079768	0.3896154196	0.2660663722
1	0.5519132871	0.3152605436	0.1717963676
1.25	0.6228576084	0.2543457448	0.1079934516
1.5	0.6800247641	0.2047028870	0.0663767004
1.75	0.7259884379	0.1644214414	0.0400411532
2	0.7628774882	0.1318523684	0.0237837569
2.25	0.7924400080	0.1055954999	0.0139493825
2.5	0.8161029111	0.0844773812	0.0080983796
2.75	0.8350253396	0.0675247036	0.0046641177
3	0.8501452547	0.0539367945	0.0026702523

Table 3. *Cont.*

η	ϵ_f	$\epsilon_{f'}$	ϵ_θ
0	$4.166664 \cdot 10^{-11}$	$5.000001 \cdot 10^{-10}$	$1.200000 \cdot 10^{-7}$
0.25	$2.338812 \cdot 10^{-9}$	$8.500138 \cdot 10^{-10}$	$5.494534 \cdot 10^{-6}$
0.5	$9.967847 \cdot 10^{-10}$	$2.982538 \cdot 10^{-8}$	$6.878355 \cdot 10^{-6}$
0.75	$4.282139 \cdot 10^{-9}$	$1.095087 \cdot 10^{-8}$	$1.161948 \cdot 10^{-6}$
1	$6.948758 \cdot 10^{-10}$	$2.880794 \cdot 10^{-8}$	$4.814365 \cdot 10^{-6}$
1.25	$4.403408 \cdot 10^{-9}$	$4.789489 \cdot 10^{-8}$	$1.652118 \cdot 10^{-7}$
1.5	$4.521325 \cdot 10^{-9}$	$1.783327 \cdot 10^{-8}$	$3.991710 \cdot 10^{-6}$
1.75	$1.352115 \cdot 10^{-9}$	$2.390061 \cdot 10^{-8}$	$2.542265 \cdot 10^{-6}$
2	$4.420232 \cdot 10^{-9}$	$6.084595 \cdot 10^{-10}$	$1.693424 \cdot 10^{-6}$
2.25	$3.888561 \cdot 10^{-9}$	$8.512293 \cdot 10^{-9}$	$5.025664 \cdot 10^{-6}$
2.5	$2.571165 \cdot 10^{-12}$	$2.233086 \cdot 10^{-8}$	$5.660951 \cdot 10^{-6}$
2.75	$4.493213 \cdot 10^{-9}$	$1.154742 \cdot 10^{-8}$	$3.836207 \cdot 10^{-6}$
3	$6.906006 \cdot 10^{-9}$	$3.618723 \cdot 10^{-9}$	$7.764704 \cdot 10^{-7}$

Table 4. Comparison between the limit-value $f(\infty) := \lim_{\eta \to \infty} f(\eta)$ obtained from Equation (31) by the OHAM and numerical results, for different values of n, γ and δ_1 (relative errors: $\epsilon_{f(\infty)} = |f_{numerical}(\infty) - \bar{f}_{OHAM}(\infty)|$).

n	γ	δ_1	$f_{numerical}(\infty)$	$\bar{f}_{OHAM}(\infty)$	$\epsilon_{f(\infty)}$
0.5	0.25	0.2	0.9946172010	0.9946172997	10^{-7}
0.5	0.25	0.5	0.9097559921	0.9097561021	10^{-7}
0.5	0.25	0.75	0.8592107287	0.8592108288	10^{-7}
0.5	0.5	0.5	0.934115512	0.93411561078	10^{-7}
0.5	1	0.5	0.984325561	0.98432566179	10^{-7}
2.5	0.25	0.5	0.754168409	0.75416850866	10^{-7}
5	0.25	0.5	0.709166712	0.70916736175	$6.496262 \cdot 10^{-7}$

For Figures 2–13, the OHAM solutions are displayed with thin lines and numerical solutions by dashing lines.

4.1. Influence of the Parameter n

The behaviour of the displacement and velocity $\bar{f}(\eta)$ and $\bar{f}'(\eta)$, respectively, with the increase in n for fixed values of $R = 1$, $Pr = 6$, $\delta_2 = 0.2$, $\gamma = 0.25$ and $\delta_1 = 0.5$, are represented in Figures 2 and 3, respectively. On the another hand from Figure 4 one can observe an increasing in temperature $\bar{\theta}(\eta)$ with n.

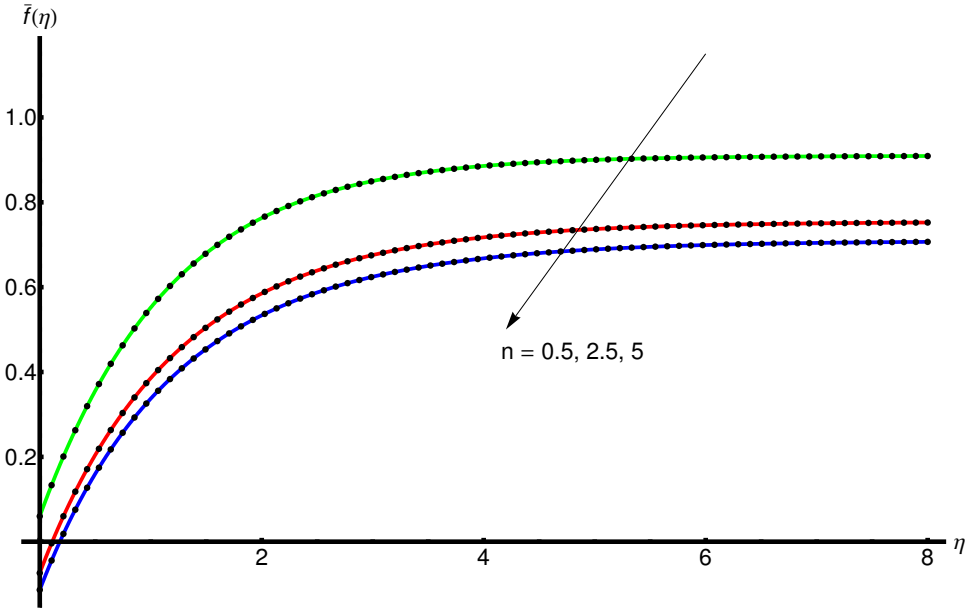

Figure 2. The influence of n on the behaviour of the displacement $\bar{f}(\eta)$ (given by Equations (A3), (A17) and (A19) for $\gamma = 0.25$, $\delta_1 = 0.5$: OHAM solution (thin lines) and numerical solution (dashing lines).

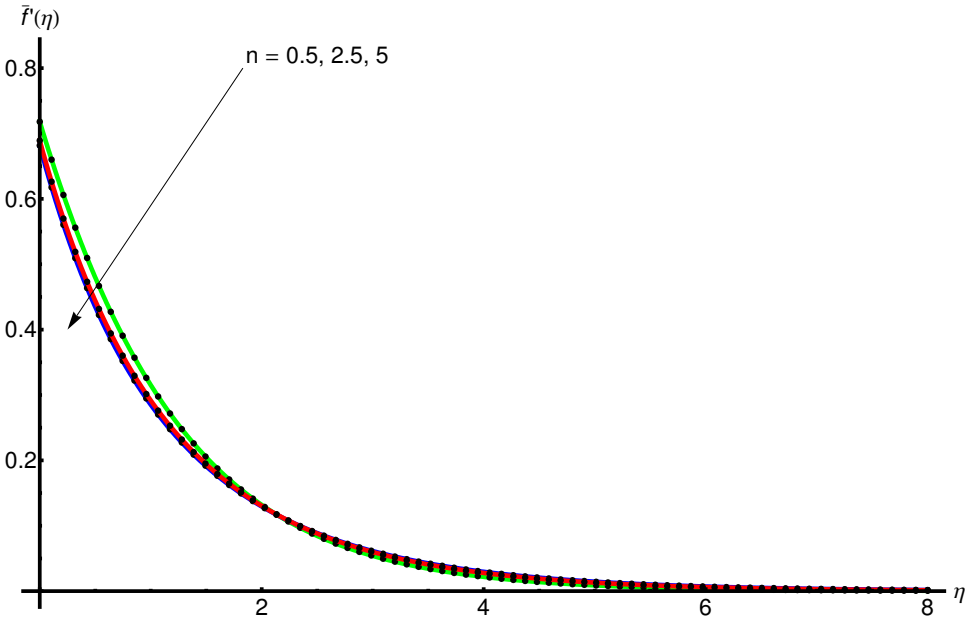

Figure 3. The influence of n on the behaviour of the velocity profile $\bar{f}'(\eta)$ obtained from Equations (A3), (A17) and (A19) for $\gamma = 0.25$, $\delta_1 = 0.5$: OHAM solution (thin lines) and numerical solution (dashing lines).

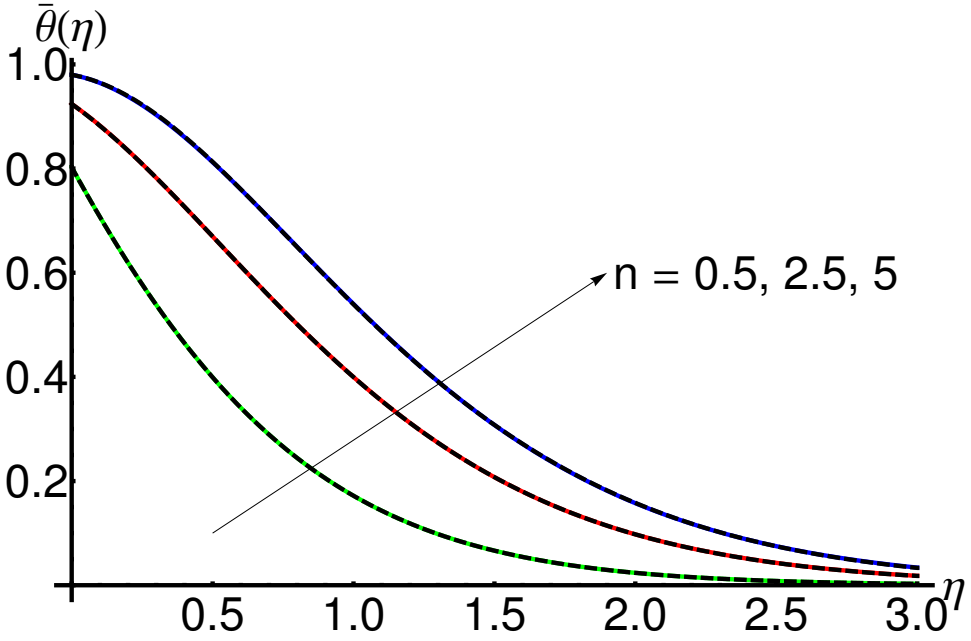

Figure 4. The influence of n on the behaviour of the temperature $\bar{\theta}(\eta)$ given by Equations (A4), (A18) and (A20) for $R = 1$, $Pr = 6$, $\delta_2 = 0.2$, $\gamma = 0.25$, $\delta_1 = 0.5$: OHAM solution (thin lines) and numerical solution (dashing lines).

The slope and asymptotic limit decreases with the increasing values of η.

4.2. Influence of the Wall Thickness Parameter γ

Figures 5 and 6 display the behaviour of the displacement $\bar{f}(\eta)$ and variation of the velocity $\bar{f}'(\eta)$, respectively, with increasing γ for fixed values of $n = 0.5$, $R = 1$, $Pr = 6$, and $\delta_2 = 0.2$, $\delta_1 = 0.5$; while Figure 7 shows the variation in the temperature $\bar{\theta}(\eta)$ decreases.

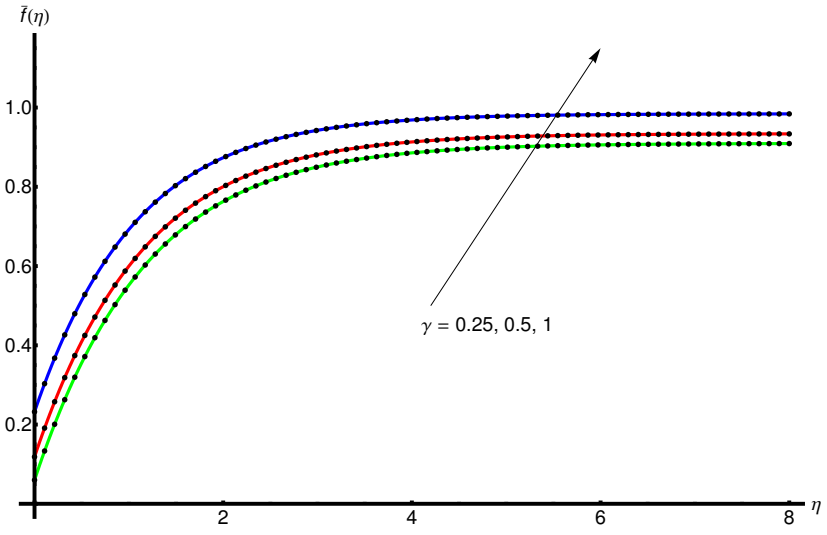

Figure 5. The influence of γ on the behaviour of the displacement $\bar{f}(\eta)$ given by Equations (A3), (A13) and (A15) for $n = 0.5$, $\delta_1 = 0.5$: OHAM solution (thin lines) and numerical solution (dashing lines).

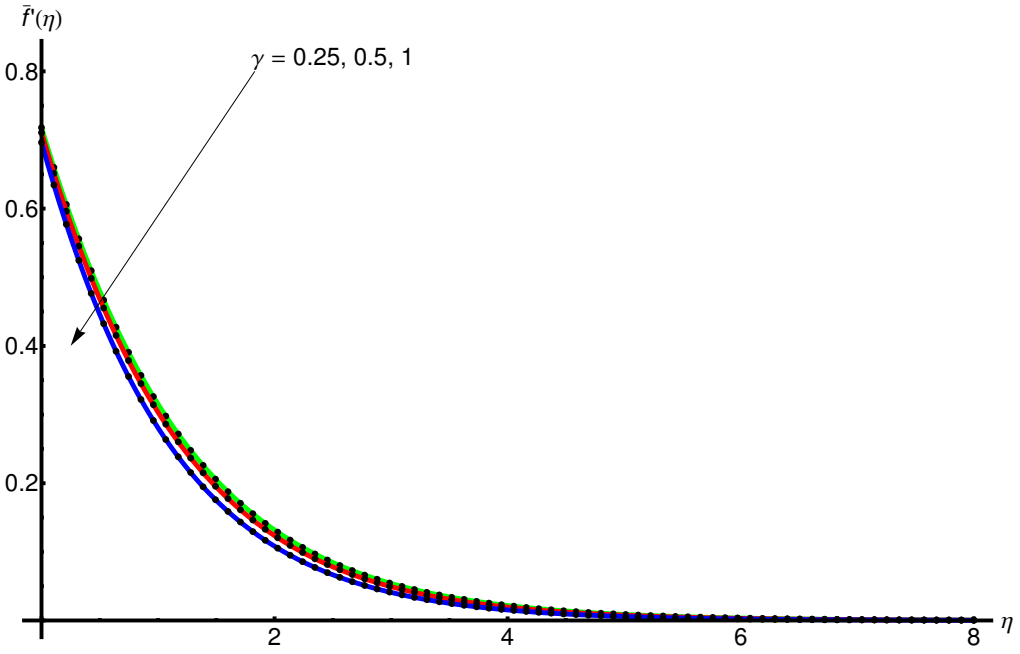

Figure 6. The influence of γ on the behaviour of the velocity profile $\bar{f}'(\eta)$ obtained from Equations (A3), (A13) and (A15) for $n = 0.5$, $\delta_1 = 0.5$: OHAM solution (thin lines) and numerical solution (dashing lines).

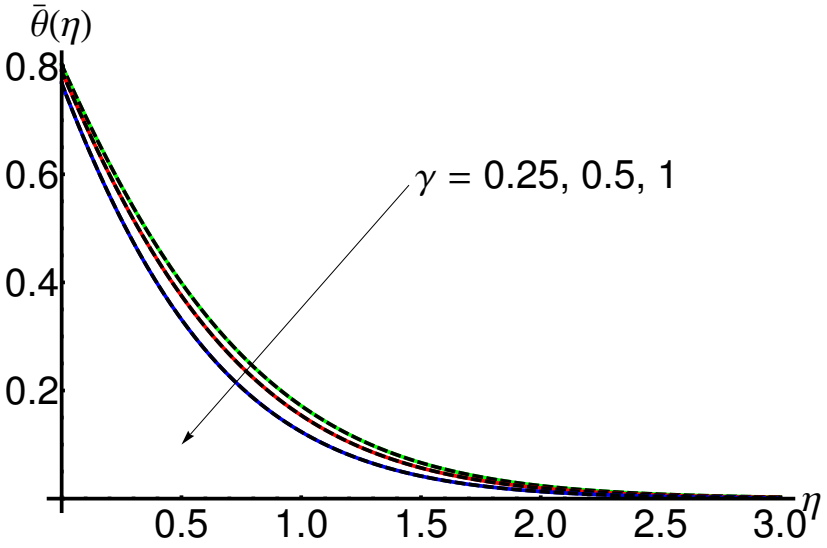

Figure 7. The influence of γ on the behaviour of the temperature $\bar{\theta}(\eta)$ given by Equations (A4), (A14) and (A16) for $n = 0.5$, $R = 1$, $Pr = 6$, $\delta_2 = 0.2$, $\delta_1 = 0.5$: OHAM solution (thin lines) and numerical solution (dashing lines).

The slope and asymptotic limit increases for increasing values of η.

4.3. Influence of the Slip Parameter δ_1

The behaviour of the displacement and velocity $\bar{f}(\eta)$ and $\bar{f}'(\eta)$, respectively with the increasing of the parameter δ_1 for some fixed values of the parameters $n = 0.5$, $R = 1$, $Pr = 6$, $\delta_2 = 0.2$, $\gamma = 0.25$, is represented in Figures 8 and 9, respectively. In the Figure 10 can be observe an increasing of the temperature $\bar{\theta}(\eta)$ with this parameter δ_1.

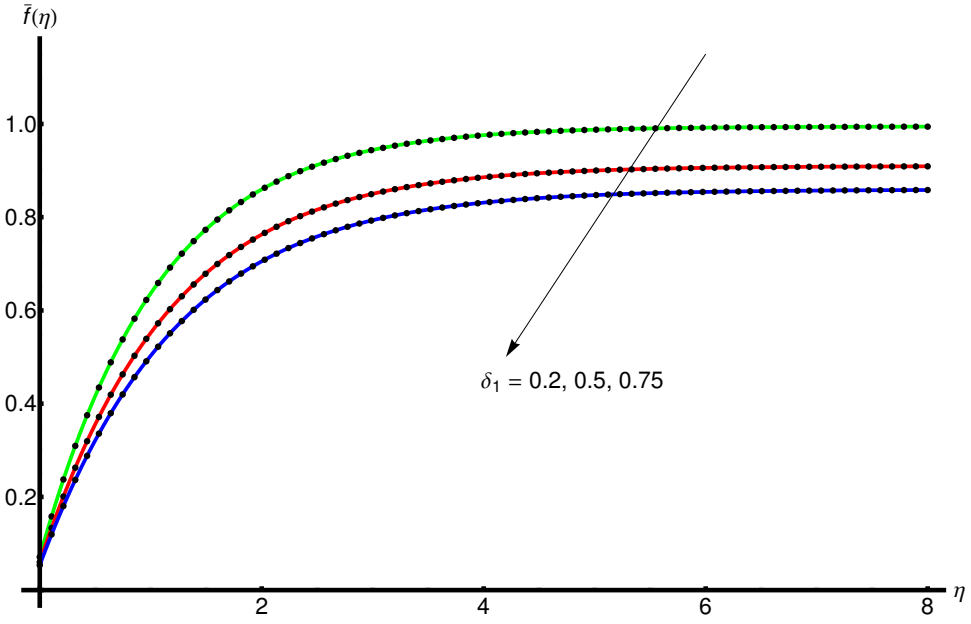

Figure 8. The influence of the parameter δ_1 on the behaviour of the displacement $\bar{f}(\eta)$ given by Equations (A1), (A3) and (A11) for $n = 0.5$, $\gamma = 0.25$: OHAM solution (thin lines) and numerical solution (dashing lines).

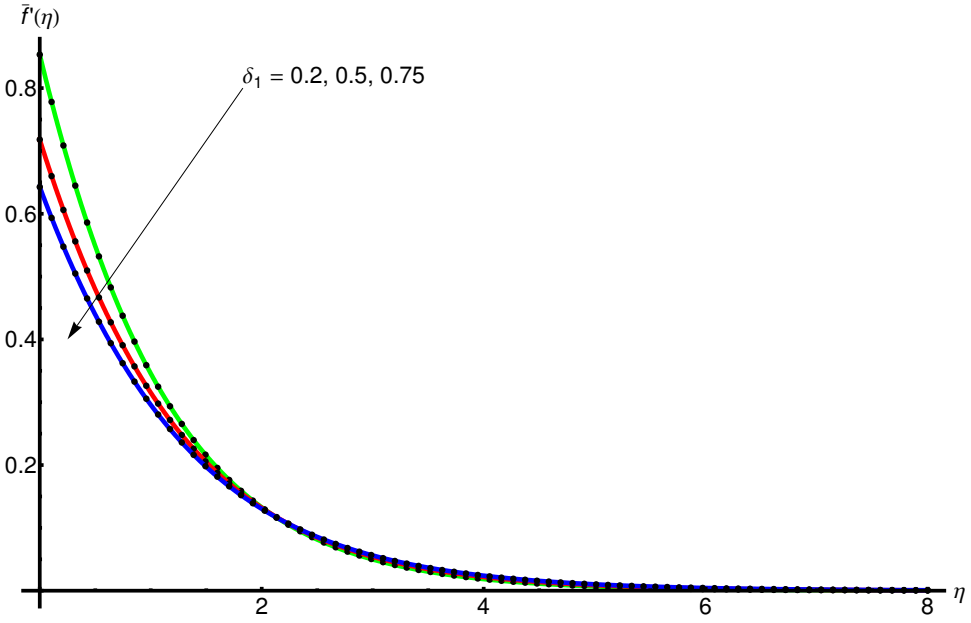

Figure 9. The influence of δ_1 on the behaviour of the velocity profile $\bar{f}'(\eta)$ obtained from Equations (A1), (A3) and (A11) for $n = 0.5$, $\gamma = 0.25$: OHAM solution (thin lines) and numerical solution (dashing lines).

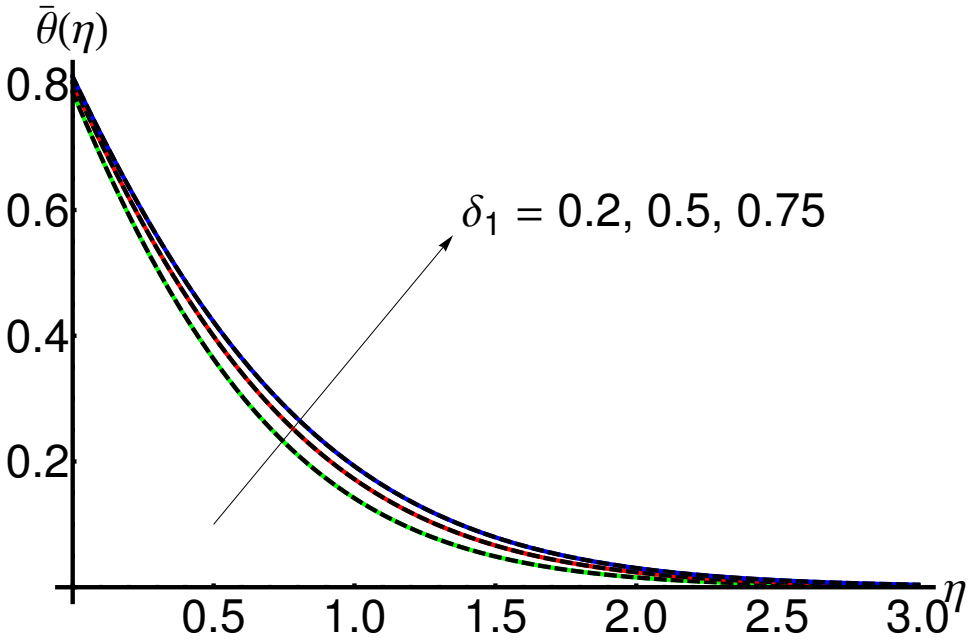

Figure 10. Profile of the temperature $\bar{\theta}(\eta)$ given by Equations (A2), (A4) and (A12) when increasing the slip parameter δ_1 for $n = 0.5$, $R = 1$, $Pr = 6$, $\delta_2 = 0.2$, $\gamma = 0.25$: OHAM solution (thin lines) and numerical solution (dashing lines).

The slope and asymptotic limit decreases for increasing values of η.

4.4. Influence of the Prandtl Number Pr

Figure 11 displays the decrease in the temperature $\bar{\theta}(\eta)$ with the increase in the Prandtl number Pr for fixed values of $n = 0.5$, $R = 1$, $\delta_2 = 0.2$, $\gamma = 0.25$, $\delta_1 = 0.5$.

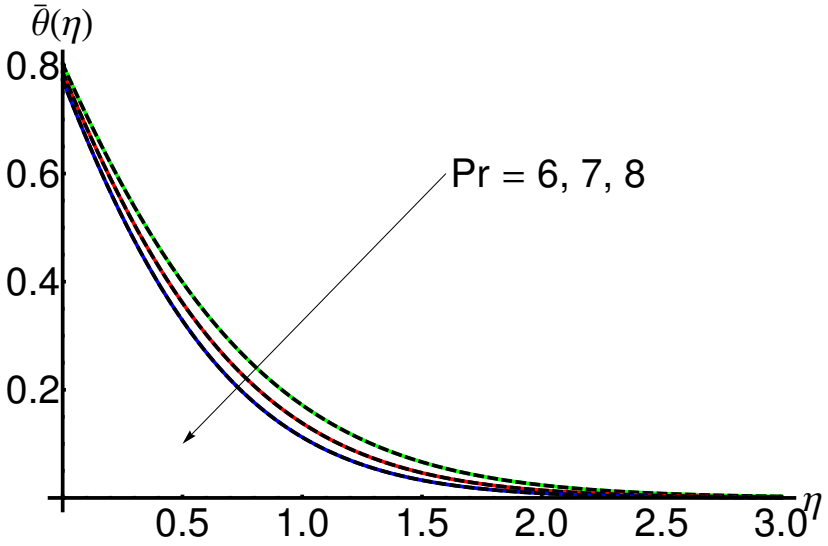

Figure 11. Profile of the temperature $\bar{\theta}(\eta)$ given by Equations (A4), (A5) and (A6) when increasing the Prandtl number Pr for $n = 0.5$, $R = 1$, $\delta_2 = 0.2$, $\gamma = 0.25$, $\delta_1 = 0.5$: OHAM solution (thin lines) and numerical solution (dashing lines).

4.5. Influence of the Radiation Parameter R

Figure 12 shows the increase in temperature $\bar{\theta}(\eta)$ when increasing the radiation number R for fixed values of $n = 0.5$, $Pr = 6$, $\delta_2 = 0.2$, $\gamma = 0.25$, $\delta_1 = 0.5$.

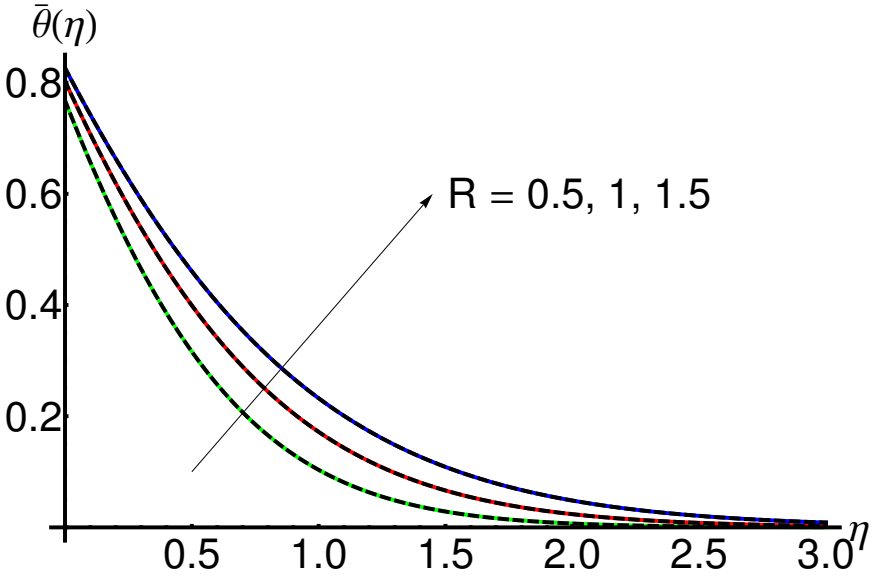

Figure 12. Profile of the temperature $\bar{\theta}(\eta)$ given by Equations (A7), (A4) and (A8) when increasing the radiation parameter R for $n = 0.5$, $Pr = 6$, $\delta_2 = 0.2$, $\gamma = 0.25$, $\delta_1 = 0.5$: OHAM solution (thin lines) and numerical solution (dashing lines).

4.6. Influence of the Slip Thermal Parameter δ_2

From Figure 13 we notice that the variation in temperature.

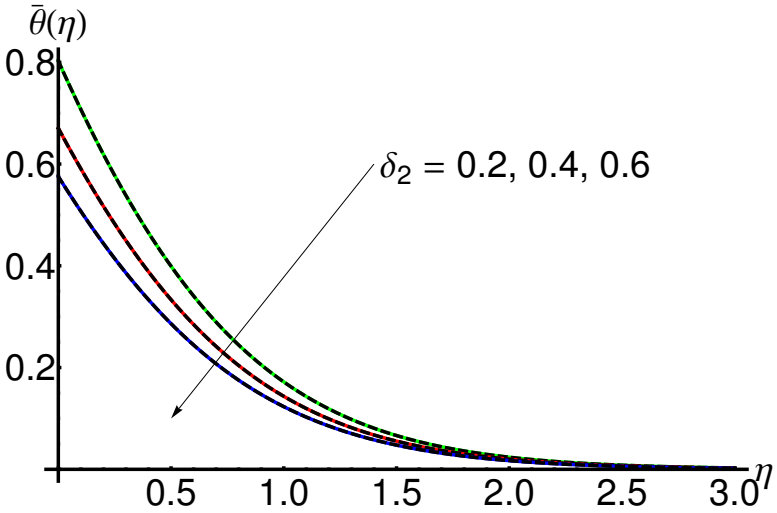

Figure 13. Profile of the temperature $\bar{\theta}(\eta)$ given by Equations (A4), (A9) and (A10) when increasing the slip thermal parameter δ_2 for $n = 0.5$, $R = 1$, $Pr = 6$, $\gamma = 0.25$, $\delta_1 = 0.5$: OHAM solution (thin lines) and numerical solution (dashing lines).

The behaviour of the temperature $\bar{\theta}(\eta)$ with increasing δ_2 for fixed values of $n = 0.5$, $R = 1$, $Pr = 6$, $\gamma = 0.25$, $\delta_1 = 0.5$ is depicted in Figure 13.

Table 5 presents in detail an error analysis by computing the integral of the square residual given by Equations (42) and (43).

Table 5. Integral of the square residual given by Equations (42) and (43) obtained by the OHAM for different values of n, γ and δ_1, R, Pr and δ_2.

n	γ	δ_1	$\int_0^\infty R_{\bar{f}}{}^2(\eta)\,d\eta$	R	Pr	δ_2	$\int_0^\infty R_{\bar{\theta}}{}^2(\eta)\,d\eta$
0.5	0.25	0.2	$5.485739 \cdot 10^{-11}$	1	6	0.2	$1.079470 \cdot 10^{-5}$
0.5	0.25	0.5	$5.503738 \cdot 10^{-13}$	1	6	0.2	$4.737834 \cdot 10^{-7}$
				1	7	0.2	$9.489441 \cdot 10^{-7}$
				1	8	0.2	$1.914615 \cdot 10^{-6}$
				0.5	6	0.2	$3.598609 \cdot 10^{-5}$
				1.5	6	0.2	$3.601433 \cdot 10^{-9}$
				1	6	0.4	$2.265013 \cdot 10^{-7}$
				1	6	0.6	$1.504156 \cdot 10^{-7}$
0.5	0.25	0.75	$2.848927 \cdot 10^{-10}$	1	6	0.2	$1.139814 \cdot 10^{-6}$
0.5	0.5	0.5	$1.486587 \cdot 10^{-11}$	1	6	0.2	$1.787740 \cdot 10^{-7}$
0.5	1	0.5	$7.256022 \cdot 10^{-11}$	1	6	0.2	$2.676813 \cdot 10^{-7}$
2.5	0.25	0.5	$2.500198 \cdot 10^{-11}$	1	6	0.2	$1.100465 \cdot 10^{-3}$
5	0.25	0.5	$3.167293 \cdot 10^{-9}$	1	6	0.2	$8.243077 \cdot 10^{-5}$

4.7. OHAM Solutions versus Iterative Solutions

A comparison between the OHAM solutions and corresponding iterative solutions obtained by the iterative method developed in [49] are presented highlighting the accuracy of the modified OHAM technique.

Equations (9) and (10) convert in the following system:

$$\begin{cases} F_1'(\eta) = F_2(\eta) \\ F_2'(\eta) = F_3(\eta) \\ F_3'(\eta) = \frac{2n}{1+n}F_2^2(\eta) - F_1(\eta)F_3(\eta) \\ \Theta_1'(\eta) = \Theta_2(\eta) \\ \Theta_2'(\eta) = \frac{Pr}{1+\frac{4}{3}R} \cdot \left(\frac{1-n}{1+n} \cdot F_2(\eta)\Theta_1(\eta) - F_1(\eta)\Theta_2(\eta)\right) \end{cases}, \tag{44}$$

where $F_1(\eta) = f(\eta)$, $F_2(\eta) = f'(\eta)$, $F_3(\eta) = f''(\eta)$, $\Theta_1(\eta) = \theta(\eta)$, $\Theta_2(\eta) = \theta'(\eta)$.

Integrating the system (44) over the interval $[0,\ \eta]$, results in:

$$\begin{aligned} F_1(\eta) &= F_1(0) + \int_0^\eta F_2(s)\,ds \\ F_2(\eta) &= F_2(0) + \int_0^\eta F_3(s)\,ds \\ F_3(\eta) &= F_3(0) + \int_0^\eta \left(\frac{2n}{1+n}F_2^2(s) - F_1(s)F_3(s)\right) ds \\ \Theta_1(\eta) &= \Theta_1(0) + \int_0^\eta \Theta_2(s)\,ds \\ \Theta_2(\eta) &= \Theta_2(0) + \int_0^\eta \frac{Pr}{1+\frac{4}{3}R} \cdot \left(\frac{1-n}{1+n} \cdot F_2(s)\Theta_1(s) - F_1(s)\Theta_2(s)\right) ds \end{aligned} \tag{45}$$

The iterative procedure leads to:

$$
\begin{aligned}
&F_{1,0}(\eta) = F_1(0)\,, \quad F_{1,1}(\eta) = N_1(F_{1,0}, F_{2,0}, F_{3,0}, \Theta_{1,0}, \Theta_{2,0}) = \int_0^\eta F_{2,0}(s)\,ds\,,\\
&F_{2,0}(\eta) = F_2(0)\,, \quad F_{2,1}(\eta) = N_2(F_{1,0}, F_{2,0}, F_{3,0}, \Theta_{1,0}, \Theta_{2,0}) = \int_0^\eta F_{3,0}(s)\,ds\,,\\
&F_{3,0}(\eta) = F_3(0)\,, \quad F_{3,1}(\eta) = N_3(F_{1,0}, F_{2,0}, F_{3,0}, \Theta_{1,0}, \Theta_{2,0}) = \int_0^\eta \Big(\frac{2n}{1+n}F_{2,0}^2(s) - F_{1,0}(s)F_{3,0}(s)\Big)\,ds\,,\\
&\Theta_{1,0}(\eta) = \Theta_1(0)\,, \quad \Theta_{1,1}(\eta) = N_4(F_{1,0}, F_{2,0}, F_{3,0}, \Theta_{1,0}, \Theta_{2,0}) = \int_0^\eta \Theta_{2,0}(s)\,ds\,,\\
&\Theta_{2,0}(\eta) = \Theta_2(0)\,, \quad \Theta_{2,1}(\eta) = N_5(F_{1,0}, F_{2,0}, F_{3,0}, \Theta_{1,0}, \Theta_{2,0}) = \int_0^\eta \frac{Pr}{1+\frac{4}{3}R}\cdot\Big(\frac{1-n}{1+n}\cdot f_{2,0}(s)\theta_{1,0}(s) - f_{1,0}(s)\theta_{2,0}(s)\Big)\,ds\,,\\
&\ldots\\
&F_{1,m}(\eta) = N_1\Big(\sum_{i=0}^{m-1}F_{1,i}, \sum_{i=0}^{m-1}F_{2,i}, \sum_{i=0}^{m-1}F_{3,i}, \sum_{i=0}^{m-1}\Theta_{1,i}, \sum_{i=0}^{m-1}\Theta_{2,i}\Big) - N_1\Big(\sum_{i=0}^{m-2}F_{1,i}, \sum_{i=0}^{m-2}F_{2,i}, \sum_{i=0}^{m-2}F_{3,i}, \sum_{i=0}^{m-2}\Theta_{1,i}, \sum_{i=0}^{m-2}\Theta_{2,i}\Big)\,,\\
&F_{2,m}(\eta) = N_2\Big(\sum_{i=0}^{m-1}F_{1,i}, \sum_{i=0}^{m-1}F_{2,i}, \sum_{i=0}^{m-1}F_{3,i}, \sum_{i=0}^{m-1}\Theta_{1,i}, \sum_{i=0}^{m-1}\Theta_{2,i}\Big) - N_2\Big(\sum_{i=0}^{m-2}F_{1,i}, \sum_{i=0}^{m-2}F_{2,i}, \sum_{i=0}^{m-2}F_{3,i}, \sum_{i=0}^{m-2}\Theta_{1,i}, \sum_{i=0}^{m-2}\Theta_{2,i}\Big)\,,\\
&F_{3,m}(\eta) = N_3\Big(\sum_{i=0}^{m-1}F_{1,i}, \sum_{i=0}^{m-1}F_{2,i}, \sum_{i=0}^{m-1}F_{3,i}, \sum_{i=0}^{m-1}\Theta_{1,i}, \sum_{i=0}^{m-1}\Theta_{2,i}\Big) - N_3\Big(\sum_{i=0}^{m-2}F_{1,i}, \sum_{i=0}^{m-2}F_{2,i}, \sum_{i=0}^{m-2}F_{3,i}, \sum_{i=0}^{m-2}\Theta_{1,i}, \sum_{i=0}^{m-2}\Theta_{2,i}\Big)\,,\\
&\Theta_{1,m}(\eta) = N_4\Big(\sum_{i=0}^{m-1}F_{1,i}, \sum_{i=0}^{m-1}F_{2,i}, \sum_{i=0}^{m-1}F_{3,i}, \sum_{i=0}^{m-1}\Theta_{1,i}, \sum_{i=0}^{m-1}\Theta_{2,i}\Big) - N_4\Big(\sum_{i=0}^{m-2}F_{1,i}, \sum_{i=0}^{m-2}F_{2,i}, \sum_{i=0}^{m-2}F_{3,i}, \sum_{i=0}^{m-2}\Theta_{1,i}, \sum_{i=0}^{m-2}\Theta_{2,i}\Big)\,,\\
&\Theta_{2,m}(\eta) = N_5\Big(\sum_{i=0}^{m-1}F_{1,i}, \sum_{i=0}^{m-1}F_{2,i}, \sum_{i=0}^{m-1}F_{3,i}, \sum_{i=0}^{m-1}\Theta_{1,i}, \sum_{i=0}^{m-1}\Theta_{2,i}\Big) - N_5\Big(\sum_{i=0}^{m-2}F_{1,i}, \sum_{i=0}^{m-2}F_{2,i}, \sum_{i=0}^{m-2}F_{3,i}, \sum_{i=0}^{m-2}\Theta_{1,i}, \sum_{i=0}^{m-2}\Theta_{2,i}\Big)\,,\\
&m \geq 2\,.
\end{aligned}
\tag{46}
$$

The solutions to Equations (9) and (10), using the iterative algorithm, can be written as:

$$
F_{1_{iter}}(\eta) = \sum_{m=0}^{\infty} F_{1,m}(t)\,,\ F_{2_{iter}}(\eta) = \sum_{m=0}^{\infty} F_{2,m}(\eta)\,,\ F_{3_{iter}}(\eta) = \sum_{m=0}^{\infty} F_{3,m}(\eta)\,,
$$

$$
\Theta_{1_{iter}}(\eta) = \sum_{m=0}^{\infty} \Theta_{1,m}(\eta)\,, \Theta_{2_{iter}}(\eta) = \sum_{m=0}^{\infty} \Theta_{2,m}(\eta)\,.
$$

The iterative solutions after six iterations and considering the initial conditions: $F_1(0) = \gamma\,\frac{1-n}{1+n}\,(1+\delta_1\cdot F_3(0))$, $F_2(0) = 1+\delta_1\cdot F_3(0)$, $F_3(0) = -0.5639692215$, $\Theta_1(0) = 1+\delta_2\cdot\Theta_2(0)$, $\Theta_2(0) = -1.0625520610$ (presented in Tables 1 and 2) and the physical constants $n = 0.5$, $\gamma = 0.25$, $\delta_1 = 0.5$, $R = 1$, $Pr = 6$, $\delta_2 = 0.2$, taking into account of the Algorithm (46), become:

$$
\begin{aligned}
&f_{1_{iter}}(\eta) = \sum_{m=0}^{6} f_{1,m}(\eta) = 0.0598346157 + 0.7180153892\eta - 0.2819846107\eta^2 +\\
&+0.0629070468\eta^3 - 0.0065651516\eta^4 - 0.0005435393\eta^5 + 0.0002673026\eta^6\,,\\
&\theta_{1_{iter}}(\eta) = \sum_{m=0}^{6} \theta_{1,m}(\eta) = 0.7874895877 - 1.0625520610\eta - 0.5312760305\eta^2 -\\
&-0.1770920101\eta^3 - 0.0442730025\eta^4 - 0.0088546005\eta^5 - 0.0014757667\eta^6\,.
\end{aligned}
\tag{47}
$$

Figures 14 and 15 and Table 6, respectively, present a parallel between the OHAM solutions $\bar{f}_{OHAM}$ and $\bar{\theta}_{OHAM}$ and the corresponding iterative solutions $f_{1_{iter}}$, $\theta_{1_{iter}}$ given in Equation (47). This comparative analysis highlights the efficiency and accuracy of the modified OHAM method using only one iteration.

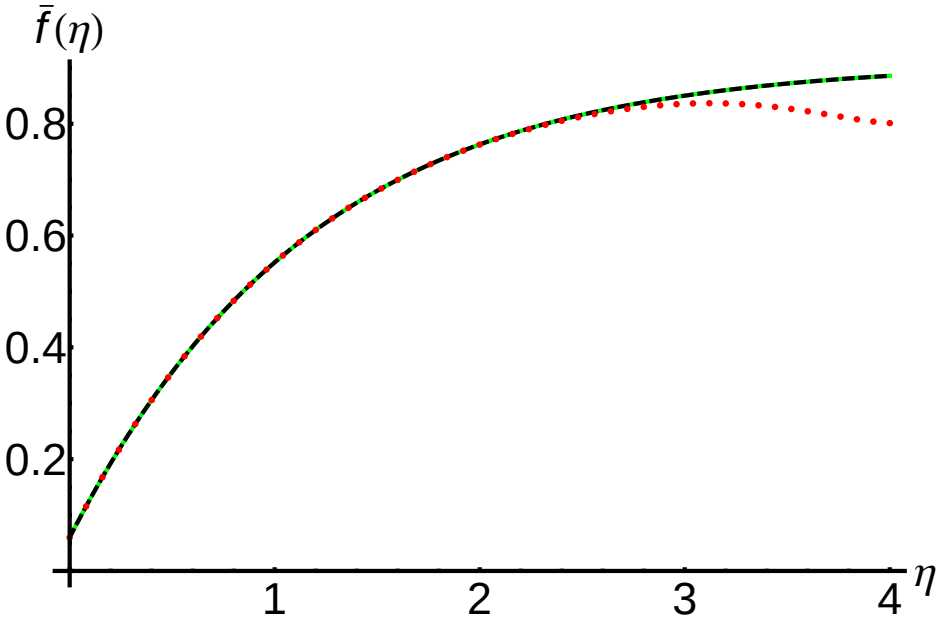

Figure 14. Profile of the approximate analytical solution $\bar{f}(\eta)$, of Equation (9) given by Equation (A3), the iterative solution $f_{1_{iter}}(\eta)$ given by Equation (47) and the corresponding numerical solution: numerical solution (thin lines), OHAM solution (dashing lines), and iterative solution (dotted curve).

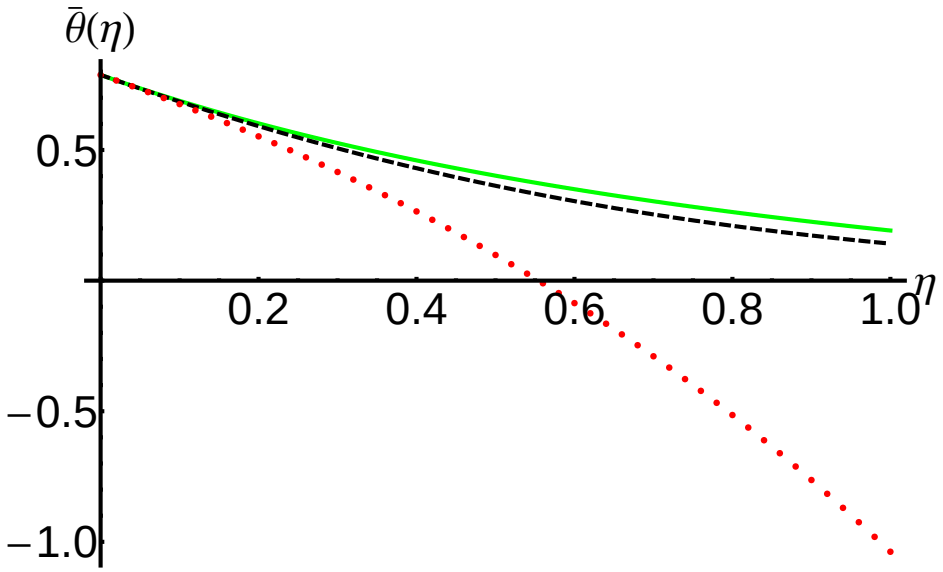

Figure 15. Profile of the approximate analytical solution $\bar{\theta}(\eta)$, of Equation (10) given by Equation (A4), the corresponding numerical solution and the iterative solution $\theta_{1_{iter}}(\eta)$ given by Equation (47). numerical solution (thin lines), OHAM solution (dashing lines), and iterative solution (dotted curve).

The precision and efficiency of the OHAM method (using just one iteration) against the iterative method described in [49] (using six iterations) arising from the presented comparison.

Table 6. Comparison between the approximate analytical solution $\bar{f}(\eta)$ given by Equation (A3), the iterative solution $f_{1_{iter}}(\eta)$ given by Equation (47) and the corresponding numerical solution.

η	$f_{numerical}$	$\bar{f}_{OHAM}$	$f_{1_{iter}}$
0	0.0598346157	0.0598346158	0.0598346157
2/5	0.3057767212	0.3057767284	0.3057767378
4/5	0.4831846866	0.4831846939	0.4831857409
6/5	0.6098618368	0.6098618446	0.6098707988
8/5	0.6996261828	0.6996261750	0.6996239146
2	0.7628775161	0.7628774882	0.7625577448
12/5	0.8072661326	0.8072660955	0.8051757704
14/5	0.8383269730	0.8383269310	0.8300974997
16/5	0.8600170821	0.8600170260	0.8362170948
18/5	0.8751415873	0.8751415052	0.8221825663
4	0.8856771883	0.8856770760	0.8010064019

5. Conclusions

Using the modified optimal homotopy asymptotic method (OHAM), the non-linear ODEs characterizing the radiative convective flow of a nanofluid over a stretching sheet in porous medium were analytically approximately solved. The equations were used to model physical phenomena related to fluid flow in the boundary layer, flow processes in porous media with applications in industry.

The dependence of the mass and heat transfer on the physical parameters was analytically and graphically investigated. The advantages of the OHAM procedure were highlighted by comparison with an iterative method. The impact of various parameters, such as: the velocity exponential factor n, the wall thickness parameter γ, the dimensionless velocity slip parameter δ_1, the Prandtl number Pr, the radiation parameter R, and the dimensionless temperature jump parameter δ_2, is presented and summarized.

- The effect of the increasing n enhances the stretching velocity and implies the elevation of the velocity boundary layer. Moreover, the temperature of the base fluid increases with n, leading the thickness of the thermal layer to increase;
- If the wall thickness parameter γ increases, then the flow characteristics are considerably reduced and the temperature gradient is lowered;
- An increase in the radiation parameter R causes an increase in the thickness of the thermal boundary layer supplying more heat to the base fluid;
- An increase in the dimensionless temperature jump parameter δ_2 generates a high surface temperature, decreasing fluid conductance and increasing the thickness of the temperature profile;
- The influence of Prandtl number Pr on the temperature field in the presence/absence of joule heating is significant. The temperature and thermal boundary layer thickness were found to decrease;
- An increase in the velocity slip parameter δ_1 implies a decrease in the boundary layer thickness, and a decrease in variation in the thermal boundary layer thickness.

The effects of the magnetic and electric fields for the radiative convective flow of a nanofluid over a stretching sheet in a porous medium will be analyzed in future work.

Author Contributions: Conceptualization, N.P.; data curation, R.-D.E. and N.P.; formal analysis, N.P.; investigation, R.-D.E. and R.B.; methodology, R.-D.E. and R.B.; software, R.-D.E.; supervision, N.P.; validation, R.-D.E. and N.P.; visualization, R.-D.E. and N.P.; writing—original draft, R.-D.E., R.B. and N.P. All authors have read and agreed to the published version of the manuscript.

Funding: This research received no external funding.

Institutional Review Board Statement: Not applicable.

Informed Consent Statement: Not applicable.

Data Availability Statement: Not applicable.

Conflicts of Interest: The authors declare no conflict of interest.

Nomenclature/Notation

Symbols	Names
$u,\ v$	Velocity components
$x,\ y$	Cartesian coordinates
n	the velocity power index parameter
$K(x)$	Non-uniform permeability
k_0	Coefficient related to non-uniform permeability
$u_w(x)$	Velocity at the wall
$T_w(x)$	Wall temperature
T_∞	Environment temperature
$u_0,\ T_0$	Reference velocity and reference temperature
A	Coefficient related to stretching sheet
ν_f	Kinematical viscosity
T	Temperature of the fluid
k	Thermal conductivity
α	Thermal diffusivity of the nanofluid
$(\rho c_p)_f$	Specific heat capacitance
δ_1^*	Dimensional velocity slip parameter
δ_2^*	Dimensional temperature jump parameter
b	the Maxwell's reflection coefficient
c	the thermal accommodation coefficient
λ	the ratio of specific heats
ξ_1, ξ_2	the mean free paths
q_r	Radiative heat flux
σ^*	the Stefan-Boltzmann constant
k^*	the mean absorption coefficient
Pr	Prandtl number
R	Radiation parameter
γ	the wall thickness parameter
δ_1	the dimensionless velocity slip parameter
δ_2	the dimensionless temperature jump parameter
Re_x	Reynolds number
η	Independent dimensionless variable
$f(\eta)$	Stream function
$\theta(\eta)$	Temperature
$\bar{f}(\eta), \bar{\theta}(\eta)$	approximate analytical solution by means of the modified Optimal Homotopy Asymptotic Method, called OHAM solutions

Appendix A

Example A1. $n = 0.5, \gamma = 0.25, \delta_1 = 0.2$

$$\begin{aligned}\bar{f}(\eta) = {} & 0.9946172997 + (0.4139772770\eta^2 - 0.6920469873\eta^3)e^{-1.8862406706\eta} + \\ & +(-0.3183621590\eta^2 + 0.0365731067\eta^3)e^{-1.1792663699\eta} + (0.1597270243\eta^2 + 0.1524443533\eta^3)\times \\ & \times e^{-1.4776951171\eta} + (-0.0042329110\eta^2 + 0.1548907491\eta^3)e^{-1.9212671996\eta} + (0.0057258538\eta^2 + \\ & +0.6348504736\eta^3)e^{-1.8637713840\eta} + (-0.2568350851\eta^2 + 0.0447155982\eta^3 - 0.0040303481\eta^4)\times \\ & \times e^{-1.2169940216\eta} + 0.1884050625e^{-1.5173282040\eta} - 1.1119121221e^{-1.0245370781\eta}\end{aligned} \tag{A1}$$

Example A1.1. $R = 1$, $Pr = 6$, $\delta_2 = 0.2$

$$\bar{\theta}(\eta) = 1.3979533623e^{-2.5662842234\eta} + (0.7874895997 - 1.6452099757\eta)e^{-1.3492902017\eta} + \\ +(-2.0002709304 - 0.2400457263\eta - 720.5014231601\eta^2)e^{-2.4345962490\eta} + (2.4384372743 + \\ +0.4502081800\eta - 0.0255707584\eta^2)e^{-1.2176022273\eta} + (-1.8361197061 - 1.3495392047\eta + \\ +719.6229654585\eta^2)e^{-2.4352044546\eta} \tag{A2}$$

Example A2. $n = 0.5$, $\gamma = 0.25$, $\delta_1 = 0.5$

$$\bar{f}(\eta) = 0.9097561021 + (-0.2869318848\eta^2 - 1.6372238807\eta^3)e^{-2.1899790308\eta} + \\ +(-0.2080549264\eta^2 - 0.7158289379\eta^3)e^{-1.7080419443\eta} + (0.1211881336\eta^2 + 0.1654718251\eta^3) \times \\ \times e^{-2.1387056347\eta} + (-0.24616933011\eta^2 + 0.6431173933\eta^3)e^{-1.7009112737\eta} + (0.08245133002\eta^2 + \\ +1.4569504253\eta^3)e^{-2.1950662752\eta} + (0.5375166777\eta^2 - 0.0782666024\eta^3 + 0.0035238270\eta^4) \times \\ \times e^{-1.4790569937\eta} + 0.0767203339e^{-1.6229736376\eta} - 0.9266418203e^{-0.9092299210\eta} \tag{A3}$$

Example A2.1. $R = 1$, $Pr = 6$, $\delta_2 = 0.2$

$$\bar{\theta}(\eta) = 2.9456787532e^{-2.7080923655\eta} + (0.8026925039 - 0.0843842327\eta)e^{-1.2290353718\eta} + \\ +(-0.2865440568 - 0.1115968792\eta - 0.9544376577\eta^2)e^{-3.4387279254\eta} + (-0.2484410860 - \\ -0.3399227766\eta - 0.0944851935\eta^2)e^{-1.7193639627\eta} + (-2.4106936104 - 0.6098471315\eta + \\ +1.3315794502\eta^2)e^{-3.1984209564\eta} \tag{A4}$$

Example A2.2. $R = 1$, $Pr = 7$, $\delta_2 = 0.2$

$$\bar{\theta}(\eta) = 1.0446433437e^{-2.8306737159\eta} + (0.7872011518 - 0.0854789194\eta)e^{-1.3516167222\eta} + \\ +(0.1496653624 + 0.0943652208\eta - 0.9855368948\eta^2)e^{-3.7177556309\eta} + (-1.2493619855 - \\ -0.0005601138\eta - 0.1324666875\eta^2)e^{-1.8588778154\eta} + (0.0550532792 + 1.3664899912\eta + \\ +2.2018621320\eta^2)e^{-3.3379348091\eta} \tag{A5}$$

Example A2.3. $R = 1$, $Pr = 8$, $\delta_2 = 0.2$

$$\bar{\theta}(\eta) = 0.1677223956e^{-2.9458417059\eta} + (0.7731817622 - 0.1092859450\eta)e^{-1.4667847122\eta} + \\ +(-1.4114699618 + 0.0170493137\eta - 0.2356907944\eta^2)e^{-2.1459838851\eta} + (0.2793534893 + \\ +2.7301443316\eta + 0.0963407657\eta^2)e^{-4.2919677703\eta} + (0.9643940768 - 0.4778722401\eta + \\ +3.2113280122\eta^2)e^{-3.6250408788\eta} \tag{A6}$$

Example A2.4. $R = 0.5$, $Pr = 6$, $\delta_2 = 0.2$

$$\bar{\theta}(\eta) = -32.5050621386e^{-2.9901539452\eta} + (0.7679197587 + 87.0878602251\eta)e^{-1.5110969515\eta} + \\ +(18.9741311586 + 1.7230004007\eta - 51.5082062592\eta^2)e^{-2.9561265117\eta} + (-6.1795235553 - \\ -83.9041335593\eta + 2.3062269196\eta^2)e^{-1.4770695180\eta} + (19.7104545354 + 3.0879025287\eta + \\ +53.8236497240\eta^2)e^{-2.9541390361\eta} \tag{A7}$$

Example A2.5. $R = 1.5$, $Pr = 6$, $\delta_2 = 0.2$

$$\bar{\theta}(\eta) = 2.7943652352e^{-2.5295926714\eta} + (0.8263731124 - 0.0440600690\eta)e^{-1.0505356777\eta} + \\ +(-3.4497097475 - 0.2372528327\eta - 0.8627823196\eta^2)e^{-2.8074987872\eta} + (-0.4491261799 - \\ -0.1800065186\eta - 0.0374528674\eta^2)e^{-1.3284417935\eta} + (1.1044706922 + 0.1826813250\eta + \\ +1.3808767029\eta^2)e^{-2.6568835870\eta} \tag{A8}$$

Example A2.6. $R = 1$, $Pr = 6$, $\delta_2 = 0.4$

$$\bar{\theta}(\eta) = 0.8867806614e^{-2.7080926564\eta} + (0.6704146128 - 0.0618716928\eta)e^{-1.2290356627\eta} + \\ +(0.1725218381 + 0.4069568146\eta - 1.2897712959\eta^2)e^{-3.3156952475\eta} + (-0.5248621360 - \\ -0.1634234046\eta - 0.0671554042\eta^2)e^{-1.6578476237\eta} + (-0.5344403636 + 0.2452221795\eta + \\ +2.0411668097\eta^2)e^{-3.1369046174\eta} \tag{A9}$$

Example A2.7. $R = 1$, $Pr = 6$, $\delta_2 = 0.6$

$$\begin{array}{l}\bar{\theta}(\eta) = 4.3111040224e^{-2.7080924834\eta} + (0.5755656406 - 0.0499255132\eta)e^{-1.2290354897\eta} + \\ +(-0.7275841885 + 0.4774478628\eta - 1.0862891617\eta^2)e^{-3.3002236696\eta} + (-0.7032195548 - \\ -0.0340863577\eta - 0.0704533764\eta^2)e^{-1.6501118348\eta} + (-2.8803002790 - 1.2930950806\eta + \\ +1.5769865882\eta^2)e^{-3.1291688285\eta}\end{array} \quad (A10)$$

Example A3. $n = 0.5$, $\gamma = 0.25$, $\delta_1 = 0.75$

$$\begin{array}{l}\bar{f}(\eta) = 0.8592108288 + (0.2070610330\eta^2 + 0.0494307555\eta^3)e^{-3.9537392065\eta} + \\ +(0.5164824390\eta^2 + 0.2578257758\eta^3)e^{-2.3181363056\eta} + (0.5799578912\eta^2 + 0.3827363388\eta^3) \times \\ \times e^{-3.1652763223\eta} + (0.6618028072\eta^2 + 0.5796957297\eta^3)e^{-2.4457198692\eta} + (0.3054908753\eta^2 + \\ +0.8309626089\eta^3)e^{-1.9160164060\eta} + (-2.2707950460\eta^2 + 0.2563475757\eta^3 - 0.0073077125\eta^4) \times \\ \times e^{-1.6292493237\eta} + 0.0771076029e^{-1.5141697991\eta} - 0.8827650793e^{-0.8602449854\eta}\end{array} \quad (A11)$$

Example A3.1. $R = 1$, $Pr = 6$, $\delta_2 = 0.2$

$$\begin{array}{l}\bar{\theta}(\eta) = 5.079842172e^{-2.7870969063\eta} + (0.8119720296 - 0.0833624724\eta)e^{-1.1578475826\eta} + \\ +(-1.8519889589 - 2.248636065\eta - 58.9934609300\eta^2)e^{-3.2639449810\eta} + (0.4053898668 - \\ -0.572633951\eta - 0.0637300121\eta^2)e^{-1.6319724905\eta} + (-3.6332430806 - 0.169372153\eta + \\ +58.7914066303\eta^2)e^{-3.2612218142\eta}\end{array} \quad (A12)$$

Example A4. $n = 0.5$, $\gamma = 0.5$, $\delta_1 = 0.5$

$$\begin{array}{l}\bar{f}(\eta) = 0.9341156107 + (-0.1390743471\eta^2 - 3.0445723243\eta^3)e^{-1.8605738407\eta} + \\ +(0.0168469051\eta^2 - 0.8833160929\eta^3)e^{-1.5746217259\eta} + (0.2980880214\eta^2 + 0.9671266866\eta^3) \times \\ \times e^{-1.8117128688\eta} + (0.3112024291\eta^2 + 1.3296964905\eta^3)e^{-1.5476443496\eta} + (1.4402441312\eta^2 + \\ +2.4376920786\eta^3)e^{-1.8668037907\eta} + (-1.9273071396\eta^2 + 0.2132086651\eta^3 - 0.0073617636\eta^4) \times \\ \times e^{-1.2752945208\eta} + 0.1911543503e^{-1.3857142064\eta} - 1.0068062970e^{-0.9690714949\eta}\end{array} \quad (A13)$$

Example A4.1. $R = 1$, $Pr = 6$, $\delta_2 = 0.2$

$$\begin{array}{l}\bar{\theta}(\eta) = 0.7923635421e^{-2.5945283111\eta} + (0.7912351664 - 0.0841178629\eta)e^{-1.3192337903\eta} + \\ +(0.0816199379 - 0.0151786345\eta - 0.3254612303\eta^2)e^{-3.6757124597\eta} + (-1.0051353710 + \\ +0.0044161888\eta - 0.1554114241\eta^2)e^{-1.8378562298\eta} + (0.1311518909 + 1.0117021785\eta + \\ +1.0256949660\eta^2)e^{-3.1131507507\eta}\end{array} \quad (A14)$$

Example A5. $n = 0.5$, $\gamma = 1$, $\delta_1 = 0.5$

$$\begin{array}{l}\bar{f}(\eta) = 0.9843256617 + (-0.4087537861\eta^2 - 1.9758523669\eta^3)e^{-2.5346694520\eta} - \\ -(0.2678754951\eta^2 - 0.0461245614\eta^3)e^{-1.3840596643\eta} + (0.1608950512\eta^2 + 0.1040290645\eta^3) \times \\ \times e^{-1.7198164890\eta} + (0.3297039955\eta^2 + 0.7559361096\eta^3)e^{-2.5769297131\eta} + (0.2142519563\eta^2 + \\ +1.2935160470\eta^3)e^{-2.4993619006\eta} + (-0.0282217218\eta^2 + 0.0034482635\eta^3 - 0.0001162653\eta^4) \times \\ \times e^{-0.9878643345\eta} + 0.0946953564e^{-1.5962582718\eta} - 0.8468678287e^{-1.0008855992\eta}\end{array} \quad (A15)$$

Example A5.1. $R = 1$, $Pr = 6$, $\delta_2 = 0.2$

$$\begin{array}{l}\bar{\theta}(\eta) = -0.3597167846e^{-2.4922451268\eta} + (0.7687126814 - 0.0954704839\eta)e^{-1.5043807923\eta} + \\ +(-0.0733310801 - 0.5892191368\eta - 0.3250643399\eta^2)e^{-4.2045319974\eta} + (0.6308197167 - \\ -0.5245411169\eta - 0.1430808772\eta^2)e^{-2.1022659987\eta} + (-0.1977718518 + 0.719415004\eta - \\ -0.0137485551\eta^2)e^{-3.0901303332\eta}\end{array} \quad (A16)$$

Example A6. $n = 2.5$, $\gamma = 0.25$, $\delta_1 = 0.5$

$$\begin{array}{l}\bar{f}(\eta) = 0.7541685086 + (0.1158185725\eta^2 - 0.4896838798\eta^3)e^{-1.4427784905\eta} - \\ -(0.2650992476\eta^2 + 0.3422872956\eta^3)e^{-1.4736158901\eta} - (0.1361159150\eta^2 + 0.0676280787\eta^3) \times \\ \times e^{-1.0977772584\eta} + (-1.3141822854\eta^2 + 0.1462983332\eta^3)e^{-0.8922579152\eta} + (-0.0555188904\eta^2 + \\ +0.7846515973\eta^3)e^{-1.4598016587\eta} + (1.6550977660\eta^2 - 0.1805368975\eta^3 + 0.0013656520\eta^4) \times \\ \times e^{-0.8898656083\eta} - 0.2844288567e^{-1.1651806024\eta} - 0.5435807934e^{-0.6581781498\eta}\end{array} \quad (A17)$$

Example A6.1. $R = 1$, $Pr = 6$, $\delta_2 = 0.2$

$$\begin{aligned}\bar{\theta}(\eta) = {} & 257.5640986648e^{-1.3008177481\eta} + (0.9240517880 - 0.0603655215\eta)e^{-0.4109521398\eta} + \\ & +(-90.7596244009 - 23.8573078674\eta - 178261.5920432491\eta^2)e^{-1.7797390335\eta} + \\ & +(-83.86711073782 + 17.9038061212\eta - 1.3679947656\eta^2)e^{-0.8898734252\eta} + \\ & +(-82.9373635260 - 42.7181083865\eta + 178250.3752803285\eta^2)e^{-1.7797468505\eta}\end{aligned} \tag{A18}$$

Example A7. $n = 5$, $\gamma = 0.25$, $\delta_1 = 0.5$

$$\begin{aligned}\bar{f}(\eta) = {} & 0.7091673617 + (1.0214662661\eta^2 - 2.2024525481\eta^3)e^{-2.2888220109\eta} + \\ & +(2.4363488175\eta^2 - 1.1479916570\eta^3)e^{-1.7177888735\eta} + (0.6130211922\eta^2 + 0.6413035628\eta^3) \times \\ & \times e^{-1.8425247246\eta} + (1.4513883678\eta^2 + 0.7195007290\eta^3)e^{-1.7920503662\eta} + (0.7683703580\eta^2 + \\ & +2.6073338327\eta^3)e^{-2.2759261623\eta} + (-6.2905950018\eta^2 + 0.6005060191\eta^3 + 0.0344934779\eta^4) \times \\ & \times e^{-1.7145828237\eta} - 0.1121579464e^{-1.5730824623\eta} - 0.7106162433e^{-0.7109424735\eta}\end{aligned} \tag{A19}$$

Example A7.1. $R = 1$, $Pr = 6$, $\delta_2 = 0.2$

$$\begin{aligned}\bar{\theta}(\eta) = {} & -200.8827425077e^{-1.8163880731\eta} + (0.9800452497 - 0.0204310992\eta)e^{-0.1018052494\eta} + \\ & +(-2.0670795815 - 0.0778464180\eta - 0.0657019518\eta^2)e^{-0.4314687029\eta} + (0.5106635013 - \\ & -0.0843065638\eta - 0.0100304601\eta^2)e^{-0.2157343514\eta} + (202.4391585879 + 25.2916387690\eta + \\ & +2.7198689180\eta^2)e^{-1.9303171751\eta}\end{aligned} \tag{A20}$$

References

1. Vishalakshi, A.B.; Maranna, T.; Shettar Mahabaleshwar, U.; Laroze, D. An Effect of MHD on Non–Newtonian Fluid Flow over a Porous Stretching/Shrinking Sheet with Heat Transfer. *Appl. Sci.* **2022**, *12*, 4937. [CrossRef]
2. Maranna, T.; Sneha, K.N.; Mahabaleshwar, U.S.; Sarris, I.E.; Karakasidis, T.E. An Effect of Radiation and MHD Newtonian Fluid over a Stretching/Shrinking Sheet with CNTs and Mass Transpiration. *Appl. Sci.* **2022**, *12*, 5466. [CrossRef]
3. Sarma, S.; Ahmed, N. Thermal Diffusion Effect on Unsteady MHD Free Convective Flow Past a Semi- Infinite Exponentially Accelerated Vertical Plate in a Porous Medium. *Can. J. Phys.* **2022**, *100*, 437–451. [CrossRef]
4. Mahabaleshwar, U.S.; Anusha, T.; Laroze, D.; Said, N.M.; Sharifpur, M. An MHD Flow of Non–Newtonian Fluid Due to a Porous Stretching/Shrinking Sheet with Mass Transfer. *Sustainability* **2022**, *14*, 7020. [CrossRef]
5. Akhtar, S.; Almutairi, S.; Nadeem, S. Impact of heat and mass transfer on the Peristaltic flow of non-Newtonian Casson fluid inside an elliptic conduit: Exact solutions through novel technique. *Chin. J. Phys.* **2022**, *78*, 194–206. [CrossRef]
6. Safdar, M.; Ijaz Khan, M.; Khan, R.A.; Taj, S.; Abbas, F.; Elattar, S.; Galal, A.M. Analytic solutions for the MHD flow and heat transfer in a thin liquid film over an unsteady stretching surface with Lie symmetry and homotopy analysis method. *Waves Random Complex Media* **2022**, *33*, 442–460. [CrossRef]
7. Krishna, M.V. Analytical study of chemical reaction, Soret, Hall and ion slip effects on MHD flow past an infinite rotating vertical porous plate. *Waves Random Complex Media* **2022**. [CrossRef]
8. Reddy, Y.D.; Mebarek-Oudina, F.; Goud, B.S.; Ismail, A.I. Radiation, Velocity and Thermal Slips Effect Toward MHD Boundary Layer Flow Through Heat and Mass Transport of Williamson Nanofluid with Porous Medium. *Arab. J. Sci. Eng.* **2022**, *47*, 16355–16369. [CrossRef]
9. Abbas, A.; Jeelani, M.B.; Alharthi, N.H. Darcy-Forchheimer Relation Influence on MHD Dissipative Third-Grade Fluid Flow and Heat Transfer in Porous Medium with Joule Heating Effects: A Numerical Approach. *Processes* **2022**, *10*, 906. [CrossRef]
10. Elbashbeshy, E.M.A.; Asker, H.G. Fluid flow over a vertical stretching surface within a porous medium filled by a nanofluid containing gyrotactic microorganisms. *Eur. Phys. J. Plus* **2022**, *137*, 541. [CrossRef]
11. Nuwairan, M.A.; Hafeez, A.; Khalid, A.; Syed, A. Heat generation/absorption effects on radiative stagnation point flow of Maxwell nanofluid by a rotating disk influenced by activation energy. *Case Stud. Therm. Eng.* **2022**, *35*, 102047. [CrossRef]
12. Abbas, N.; UrRehman, K.; Shatanawi, W.; Malik, M.Y. Numerical study of heat transfer in hybrid nanofluid flow over permeable nonlinear stretching curved surface with thermal slip. *Int. Commun. Heat Mass Transf.* **2022**, *135*, 106107. [CrossRef]
13. Hossein, S.; Ahmadi, N.; Jabbary, A. Effects of applying brand-new designs on the performance of PEM fuel cell and water flooding phenomena. *Iran. J. Chem. Chem. Eng.* **2022**, *41*, 618–634.
14. Aziz, T.; Aziz, A.; Shams, M.; Bahaidarah, H.M.S.; Alie, H. Entropy analysis with the Cattaneo-Christov heat flux model for the Powell-Eyring nanofluid flow over a stretching surface. *Waves Random Complex Media* **2022**. [CrossRef]
15. Jena, S.; Mishra, S.R.; Aghaeiboorkheili, M.; Pattnaik, P.K.; Muduli, K. Impact of Newtonian heating on the conducting Casson fluid flow past a stretching cylinder. *J. Interdiscip. Math.* **2022**, *25*, 2401–2416. [CrossRef]
16. Sultana, U.; Mushtaq, M.; Muhammad, T. Numerical simulation for stagnation-point flow of nanofluid over a spiraling disk through porous media. *Waves Random Complex Media* **2022**. [CrossRef]
17. Gul, T.; Saeed, A. Nonlinear mixed convection couple stress tri-hybrid nanofluids flow in a Darcy-Forchheimer porous medium over a nonlinear stretching surface. *Waves Random Complex Media* **2022**. [CrossRef]

18. Khan, M.R.; Algarni, S.; Alqahtani, T.; Alsallami, S.A.M.; Saeed, T.; Galal, A.M. Numerical analysis of a time-dependent aligned MHD boundary layer flow of a hybrid nanofluid over a porous radiated stretching/shrinking surface. *Waves Random Complex Media* **2022**. [CrossRef]
19. Rasool, G.; Shah, N.A.; El-Zahar, E.R.; Wakif, A. Numerical investigation of EMHD nanofluid flows over a convectively heated riga pattern positioned horizontally in a Darcy-Forchheimer porous medium: Application of passive control strategy and generalized transfer laws. *Waves Random Complex Media* **2022**. [CrossRef]
20. Reddy, P.B.A.; Jakeer, S.; Basha, H.T.; Reddy, S.R.; Kumar, T.M. Multi-layer artificial neural network modeling of entropy generation on MHD stagnation point flow of Cross-nanofluid. *Waves Random Complex Media* **2022**. [CrossRef]
21. Fadaei, M.; Izadi, M.; Assareh, E.; Ershadi, A. Melting process of PCM with Carreau—Yasuda non-Newtonian behavior in a shell and tube heat exchanger occupied by anisotropic porous medium. *Int. J. Numer. Heat Fluid Flow* 2022, *ahead-of-print*. [CrossRef]
22. Wang, J.; Mustafa, Z.; Siddique, I.; Ajmal, M.; Jaradat, M.M.M.; Rehman, S.U.; Ali, B.; Muhammad Ali, H. Computational Analysis for Bioconvection of Microorganisms in Prandtl Nanofluid Darcy-Forchheimer Flow across an Inclined Sheet. *Nanomaterials* **2022**, *12*, 1791. [CrossRef] [PubMed]
23. Abdal, S.; Siddique, I.; Din, I.S.U.; Ahmadian, A.; Hussain, S.; Salimi, M. Significance of magnetohydrodynamic Williamson Sutterby nanofluid due to a rotating cone with bioconvection and anisotropic slip. *J. Appl. Math. Mech.* **2022**, *102*, e202100503. [CrossRef]
24. Wahid, N.S.; Arifin, N.; Khashi'Ie, N.S.; Pop, I.; Bachok, N.; Hafidzuddin, M.E.H. Hybrid nanofluid stagnation point flow past a slip shrinking Riga plate. *Chin. J. Phys.* **2022**, *78*, 180–193. [CrossRef]
25. Meenakumari, R.; Lakshminarayana, P. MHD 3D flow of powell eyring fluid over a bidirectional non-linear stretching surface with temperature dependent conductivity and heat absorption/generation. *Proc. Inst. Mech. Eng. Part E J. Process Mech. Eng.* **2022**, *236*, 2580–2588. [CrossRef]
26. Alharbi, K.A.M.; Khan, M.R.; Ould Sidi, M.; Algelany, A.M.; Elattar, S.; Ahammad, N.A. Investigation of hydromagnetic bioconvection flow of Oldroyd-B nanofluid past a porous stretching surface. *Biomass Convers. Biorefin.* **2022**, *13*, 4331–4342. [CrossRef]
27. Krishna, M.; Vajravelu, K. Rotating MHD flow of second grade fluid through porous medium between two vertical plates with chemical reaction, radiation absorption, Hall, and ion slip impacts. *Biomass Convers. Biorefin.* **2022**. [CrossRef]
28. Tayebi, T. Analysis of the local non-equilibria on the heat transfer and entropy generation during thermal natural convection in a non-Darcy porous medium. *Int. Commun. Heat Mass Transf.* **2022**, *135*, 106133. [CrossRef]
29. Zainal, N.A.; Nazar, R.; Naganthran, K.; Pop, I. Stability Analysis of Unsteady Hybrid Nanofluid Flow over the Falkner-Skan Wedge. *Nanomaterials* **2022**, *12*, 1771. [CrossRef]
30. Jha, B.; Samaila, G. Similarity solution for boundary layer flow near a moving vertical porous plate with combined effects of nonlinear thermal radiation and suction/injection having convective surface boundary condition. *Proc. Inst. Mech. Eng. J. Mech. Eng. Sci.* **2022**, *236*, 8926–8934. [CrossRef]
31. Meena, O.P.; Janapatla, P. Mixed convection flow over a vertical cone saturated porous medium with double dispersion effect. *Appl. Math. Comput.* **2022**, *430*, 127072. [CrossRef]
32. Naseem, T.; Fatima, U.; Munir, M.; Shahzad, A.; Kausar, N.; Nisar, K.S.; Saleel, C.A.; Abbas, M. Joule heating and viscous dissipation effects in hydromagnetized boundary layer flow with variable temperature. *Case Stud. Therm. Eng.* **2022**, *35*, 102083. [CrossRef]
33. Veeram, G.; Poojitha, P.; Katta, H.; Hemalatha, S.; Babu, M.J.; Raju, C.S.; Shah, N.A.; Yook, S.J. Simulation of Dissipative Hybrid Nanofluid (PEG-Water + ZrO2 + MgO) Flow by a Curved Shrinking Sheet with Thermal Radiation and Higher Order Chemical Reaction. *Mathematics* **2022**, *10*, 1706. [CrossRef]
34. Kumar, G.V.; Rehman, K.U.; Kumar, R.V.M.S.S.K.; Shatanawi, W. Unsteady magnetohydrodynamic nanofluid flow over a permeable exponentially surface manifested with non-uniform heat source/sink effects. *Waves Random Complex Media* **2022**. [CrossRef]
35. Rooman, M.; Jan, M.A.; Shah, Z.; Vrinceanu, N.; Bou, S.F.; Iqbal, S.; Deebani, W. Entropy Optimization on Axisymmetric Darcy-Forchheimer Powell-Eyring Nanofluid over a Horizontally Stretching Cylinder with Viscous Dissipation Effect. *Coatings* **2022**, *12*, 749. [CrossRef]
36. Goud, B.S.; Reddy, Y.D.; Mishra, S. Joule heating and thermal radiation impact on MHD boundary layer Nanofluid flow along an exponentially stretching surface with thermal stratified medium. *Proc. Inst. Mech. Eng. J. Nanomater. Nanoeng. Nanosyst.* **2022**, 23977914221100961. [CrossRef]
37. Manvi, B.; Tawade, J.; Biradar, M.; Noeiaghdam, S.; Fernandez-Gamiz, U.; Govindan, V. The effects of MHD radiating and non-uniform heat source/sink with heating on the momentum and heat transfer of Eyring-Powell fluid over a stretching. *Results Eng.* **2022**, *14*, 100435. [CrossRef]
38. Ali, A.; Khan, H.S.; Saleem, S.; Hussan, M. EMHD Nanofluid Flow with Radiation and Variable Heat Flux Effects along a Slandering Stretching Sheet. *Nanomaterials* **2022**, *12*, 3872. [CrossRef]
39. Marinca V.; Herisanu N. *The Optimal Homotopy Asymptotic Method—Engineering Applications*; Springer: Berlin/Heidelberg, Germany, 2015.
40. Marinca, V.; Ene, R.D.; Marinca, B.; Negrea, R. Different approximations to the solution of upper-convected Maxwell fluid over a porous stretching plate. *Abstr. Appl. Anal.* **2014**, *2014*, 139314. [CrossRef]

41. Ene, R.D.; Marinca, V. Approximate solutions for steady boundary layer MHD viscous flow and radiative heat transfer over an exponentially porous stretching sheet. *Appl. Math. Comput.* **2015**, *269*, 389–401. [CrossRef]
42. Ene, R.D.; Szabo, M.A.; Danoiu, S. Viscous flow and heat transfer over a permeable shrinking sheet with partial slip. *Mater. Plast.* **2015**, *52*, 408–412.
43. Marinca, V.; Ene, R.D. Dual approximate solutions of the unsteady viscous flow over a shrinking cylinder with Optimal Homotopy Asymptotic Method. *Adv. Math. Phys.* **2014**, *2014*, 417643. [CrossRef]
44. Ene, R.D.; Pop, N. Dual approximate solutions for the chemically reactive solute transfer in a viscous fluid flow. *Waves Random Complex Media* **2022**, 1–23. [CrossRef]
45. Ene, R.D.; Petrisor, C. Some mathematical approaches on the viscous flow problem on a continuous stretching surface: Nonlinear stability and dual approximate analytic solutions. *AIP Conf. Proc.* **2020**, *2293*, 350004.
46. Devi, S.P.A.; Thiyagarajan, M. Steady nonlinear hydromagnetic flow and heat transfer over a stretching surface of variable temperature. *Heat Mass Transf.* **2006**, *42*, 671–677. [CrossRef]
47. Sulochana, C.; Sandeep, N. Dual Solutions for Radiative MHD Forced Convective Flow of a Nanofluid over a Slendering Stretching Sheet in Porous Medium. *J. Nav. Archit. Mar. Eng.* **2015**, *12*, 115–124. [CrossRef]
48. Brewster, M.Q. *Thermal Radiative Transfer Properties*; John Wiley and Sons: Hoboken, NJ, USA, 1972.
49. Daftardar-Gejji, V.; Jafari, H. An iterative method for solving nonlinear functional equations. *J. Math. Anal. Appl.* **2006**, *316*, 753–763. [CrossRef]